Breakdown of Fermi liquid theory in topological multi-Weyl semimetals

Jing-Rong Wang,[1] Guo-Zhu Liu,[2,*] and Chang-Jin Zhang[1,3,†]

[1]*Anhui Province Key Laboratory of Condensed Matter Physics at Extreme Conditions,*
High Magnetic Field Laboratory of the Chinese Academy of Science, Hefei, Anhui 230031, China
[2]*Department of Modern Physics, University of Science and Technology of China, Hefei, Anhui 230026, China*
[3]*Institute of Physical Science and Information Technology, Anhui University, Hefei, Anhui 230601, China*

Fermi liquid theory works very well in most normal metals, but is found violated in many strongly correlated electron systems, such as cuprate and heavy-fermion superconductors. A widely accepted criterion is that the Fermi liquid theory is valid when the interaction-induced fermion damping rate approaches zero more rapidly than the energy. Otherwise, it is invalid. Here, we demonstrate that this criterion breaks down in topological double- and triple-Weyl semimetals. Renormalization group analysis reveals that, although the damping rate of double- and triple-Weyl fermions induced by the Coulomb interaction approaches zero more rapidly than the energy, the quasiparticle residue vanishes and the Fermi liquid theory is invalid. This behavior indicates a weaker-than-marginal violation of the Fermi liquid theory. Such an unconventional non-Fermi liquid state originates from the special dispersion of double- and triple-Weyl fermions, and is qualitatively different from all the other Fermi liquid and non-Fermi liquid states. The predicted properties of the fermion damping rate and the spectral function can be probed by the angle-resolved photoemission spectroscopy. The density of states, specific heat, and conductivities are also calculated and analyzed after incorporating the corrections induced by the Coulomb interaction.

I. INTRODUCTION

Fermi liquid (FL) theory [1,2], originally proposed by Landau, provides a qualitatively correct and even quantitatively precise description of a plethora of interacting fermion systems. In a FL, the interaction-induced fermion damping becomes progressively unimportant as the energy is lowered. The fermionic excitations are long lived near the Fermi surface, and can be described by the model of free-fermion gas. Usually, the only quantum many-body effect is the regular renormalization of a few number of parameters, such as the fermion mass, which greatly simplifies theoretical treatment.

To judge whether the FL theory is applicable in an interacting fermion system, one needs to first develop an effective criterion. The interparticle interaction leads to a fermion damping rate, defined as $\Gamma(\omega) = |\mathrm{Im}\Sigma^R(\omega)|$, where $\mathrm{Im}\Sigma^R(\omega)$ is the imaginary part of retarded fermion self-energy [1–4]. Pauli's exclusion principle guarantees that $\Gamma(\omega)$ must vanish at the Fermi surface, namely, $\Gamma(\omega \to 0) \to 0$. However, $\Gamma(\omega)$ might go to zero quickly or slowly, depending on the nature and the strength of the interparticle interaction. According to the traditional quantum many-body theory, the FL theory is valid if the fermion damping rate approaches to zero more rapidly than the energy ω in the limit $\omega \to 0$ [4], namely,

$$\lim_{\omega \to 0} \frac{\Gamma(\omega)}{\omega} \to 0. \tag{1}$$

*Corresponding author: gzliu@ustc.edu.cn
†Corresponding author: zhangcj@hmfl.ac.cn

If this criterion is not satisfied, the fermion damping is believed to be strong enough to destroy the coherent quasiparticles, leading to the breakdown of FL description [3,4].

In ordinary metals, the Coulomb interaction is short ranged due to Debye screening, and only causes weak damping. It is well established [1–4] that the fermion damping rate behaves as $\Gamma(\omega) \propto \omega^2$ in three-dimensional (3D) metals and $\Gamma(\omega) \propto \omega^2 \ln(\omega_0/\omega)$ in two-dimensional (2D) metals, respectively. In both cases, the criterion (1) is satisfied, and the FL theory works well. When fermions couple to some gapless bosonic mode, such as U(1) gauge boson [5,6] or the quantum critical fluctuation of a local order parameter [7–11], the damping rate might take the form $\Gamma(\omega) \propto \omega^a$ with $0 < a \leqslant 1$. For instance, the damping rate is $\Gamma(\omega) \propto \omega^{2/3}$ at the ferromagnetic (FM) quantum critical point (QCP) [4,8] and nematic QCP [9], and $\Gamma(\omega) \propto \omega^{1/2}$ at the antiferromagnetic (AFM) QCP [7,8]. When $0 < a \leqslant 1$, the criterion (1) is no longer satisfied and the FL theory becomes invalid. The case of $a = 1$ is very special and defines a marginal Fermi liquid (MFL) [4,12,13], which offers a good phenomenological description of the unusual normal state of cuprate superconductors. In a MFL, $\Gamma(\omega)$ and ω approach to zero in the same way. MFL has long been regarded as the weakest imaginable violation of FL theory [4,12,14,15].

Although the criterion (1) has been commonly used to judge whether or not the FL theory is valid in all the previously studied fermion systems, we will demonstrate in this paper that this criterion is not always efficient. Remarkably, we find that this criterion breaks down in both double- and triple-Weyl semimetals (WSMs), which carry multiple monopole

charges and are thus topologically nontrivial [16–44]. In these two types of semimetal (SM), the valence and conduction bands touch only at isolated points. When the Fermi level is adjusted to the band-touching points, the fermion density of states (DOS) vanishes and the Coulomb interaction remains long ranged. Owing to the special dispersion of double- and triple-Weyl fermions, the Coulomb interaction may induce highly unusual low-energy behaviors that do not occur in other interacting fermion systems. To address this issue, we perform a renormalization group (RG) analysis [45] beyond the instantaneous approximation to obtain the scale dependence of all the model parameters. The fermion damping rate $\Gamma(\omega)$ obtained in our RG analysis satisfies the criterion (1), thus the Landau damping of double- and triple-Weyl fermions is weaker than that of MFL. Based on the traditional criterion, one would naively conclude that the FL theory is valid. This is actually incorrect. Indeed, we find that the quasiparticle residue Z_f decreases all the way upon approaching to the Fermi level, albeit at a small speed. In the zero-energy limit, Z_f vanishes. Obviously, there is no overlap between the interacting and free fermions, and both double- and triple-WSMs exhibit an unconventional non-FL ground state. This non-FL state is qualitatively distinct from all the other FLs and non-FLs, and provides an example of weaker-than-marginal violation of the FL theory.

We thus see that the widely adopted criterion for the validity of FL theory is actually incomplete. It is necessary to develop a more complete formalism to define and classify non-FL states. The unconventional violation of FL theory originates from the special energy dispersion of fermions in double- and triple-WSMs. Our work provides important insight into the intriguing quantum many-body effects.

The unconventional non-FL state predicted in this work is experimentally detectable. The damping rate and spectral function of double- and triple-Weyl fermions exhibit unique and distinguishable features, which could be explored by performing angle-resolved photoemission spectroscopy (ARPES) experiments [46–54] in several candidate double- and triple-WSM materials, provided that the system is tuned close to the band-touching point. Moreover, the fermion DOS, specific heat, and conductivities can also be used to characterize such a non-FL state. We will calculate these observable quantities and analyze the interaction corrections.

The rest of the paper will be organized as follows. The model Hamiltonian and the propagators for Weyl fermions are described in Sec. II. In Sec. III, we present the coupled RG flow equations for the model parameters, and analyze the numerical results. On the basis of the solutions, we demonstrate that double- and triple-Weyl fermions exhibit unconventional non-FL behaviors, which is distinct from all the other types of fermion. We then calculate a number of observable quantities in Sec. IV and analyze their low-energy properties. We discuss how to experimentally probe the observable effects of the non-FL state and give a brief remark on the impact of finite chemical potential in Sec. V. We summarize the main results of this paper and compare to previous relevant works in Sec. VI. All the computational details are presented in Appendices A–F.

II. MODEL HAMILTONIAN

The Hamiltonian for free double-Weyl fermions is

$$H_d = \sum_{j=1}^{N} \int d^3\mathbf{x}\, \psi_{d,j}^\dagger(\mathbf{x}) \mathcal{H}_d(\mathbf{x}) \psi_{d,j}(\mathbf{x}),$$

$$\mathcal{H}_d(\mathbf{x}) = A d_1(\mathbf{x})\sigma_x + A d_2(\mathbf{x})\sigma_y + v d_3(\mathbf{x})\sigma_z, \tag{2}$$

where $d_1(\mathbf{x}) = -(\partial_x^2 - \partial_y^2)$, $d_2(\mathbf{x}) = -2\partial_x \partial_y$, and $d_3(\mathbf{x}) = -i\partial_z$. The Hamiltonian for the free triple-Weyl fermions is written as

$$H_t = \sum_{j=1}^{N} \int d^3\mathbf{x}\, \psi_{t,j}^\dagger(\mathbf{x}) \mathcal{H}_t(\mathbf{x}) \psi_{t,j}(\mathbf{x}),$$

$$\mathcal{H}_t(\mathbf{x}) = B g_1(\mathbf{x})\sigma_x + B g_2(\mathbf{x})\sigma_y + v g_3(\mathbf{x})\sigma_z, \tag{3}$$

where $g_1(\mathbf{x}) = i(\partial_x^3 - \partial_x \partial_y^2)$, $g_2(\mathbf{x}) = i(\partial_y^3 - \partial_y \partial_x^2)$, and $g_3(\mathbf{x}) = -i\partial_z$. Here, we use $\psi_{d,j}$ and $\psi_{t,j}$ to represent the two-component spinor fields for double- and triple-Weyl fermions, respectively. The index j is $j = 1, 2, \ldots, N$ with N being the number of fermion flavor. $\sigma_{x,y,z}$ are the standard Pauli matrices. Two model parameters A and v are introduced to characterize the spectrum of double-Weyl fermions, satisfying

$$E_d(\mathbf{k}) = \sqrt{A^2 k_\perp^4 + v^2 k_z^2}. \tag{4}$$

The energy spectrum of triple-Weyl fermions is given by

$$E_t(\mathbf{k}) = \sqrt{B^2 k_\perp^6 + v^2 k_z^2}, \tag{5}$$

where B is another independent model parameter. For double- and triple-Weyl fermions, the monopole charges are known to be ± 2 and ± 3 [16–44], respectively. As a comparison, the monopole changes are ± 1 for usual Weyl fermions [16]. The interesting topological properties of double- and triple-WSMs are directly related to the above fermion dispersions.

The fermions are subject to the long-range Coulomb interaction, which is described by

$$H_C = \frac{1}{4\pi} \sum_{j=1}^{N} \int d^3\mathbf{x}\, d^3\mathbf{x}'\, \rho_j(\mathbf{x}) \frac{e^2}{\epsilon |\mathbf{x} - \mathbf{x}'|} \rho_j(\mathbf{x}'), \tag{6}$$

where the fermion density operator is given by $\rho_j(\mathbf{x}) = \psi_j^\dagger(\mathbf{x})\psi_j(\mathbf{x})$. We use e to denote electron charge and ϵ dielectric constant. The total model will be treated by making perturbative expansion in powers of $1/N$.

The free propagator of double-Weyl fermions reads as

$$G_{d0}(i\omega, \mathbf{k}) = \frac{1}{i\omega - A d_1(\mathbf{k})\sigma_x - A d_2(\mathbf{k})\sigma_y - v k_z \sigma_z}, \tag{7}$$

where $d_1(\mathbf{k}) = (k_x^2 - k_y^2)$ and $d_2(\mathbf{k}) = 2k_x k_y$, and the free propagator of triple-Weyl fermions is

$$G_{t0}(i\omega, \mathbf{k}) = \frac{1}{i\omega - B g_1(\mathbf{k})\sigma_x - B g_2(\mathbf{k})\sigma_y - v k_z \sigma_z}, \tag{8}$$

where $g_1(\mathbf{k}) = (k_x^3 - 3k_x k_y^2)$ and $g_2(\mathbf{k}) = (k_y^3 - 3k_y k_x^2)$. Independent of fermion dispersion, the bare Coulomb interaction function has the form in momentum space

$$V_0(\mathbf{q}) = \frac{4\pi e^2}{\epsilon (q_\perp^2 + \zeta q_z^2)} = \frac{4\pi \alpha v}{q_\perp^2 + \zeta q_z^2}, \qquad (9)$$

where $\alpha = e^2/\epsilon v$ serves as an effective interaction strength. Since the fermion dispersion is anisotropic, the momentum components $q_\perp$ and q_z should be rescaled differently under RG transformations. To facilitate RG calculation, we introduce the parameter ζ and require that $q_\perp$ and $\sqrt{\zeta} q_z$ scale in the same way. After including the dynamical screening caused by the polarization function, one can write the dressed Coulomb interaction function as

$$V_{d,t}(i\Omega, \mathbf{q}) = \frac{1}{V_0^{-1}(\mathbf{q}) + \Pi_{d,t}(i\Omega, \mathbf{q})}, \qquad (10)$$

in which the polarization functions for double- and triple-Weyl fermions are defined as

$$\Pi_d(i\Omega, \mathbf{q}) = -N \int \frac{d\omega}{2\pi} \frac{d^3\mathbf{k}}{(2\pi)^3} \mathrm{Tr}[G_{d0}(i\omega, \mathbf{k}) G_{d0}(i\omega + i\Omega, \mathbf{k} + \mathbf{q})] \qquad (11)$$

and

$$\Pi_t(i\Omega, \mathbf{q}) = -N \int \frac{d\omega}{2\pi} \frac{d^3\mathbf{k}}{(2\pi)^3} \mathrm{Tr}[G_{t0}(i\omega, \mathbf{k}) G_{t0}(i\omega + i\Omega, \mathbf{k} + \mathbf{q})]. \qquad (12)$$

These two functions are computed in Appendix A. They can be well approximated by the following analytical expressions:

$$\Pi_d(i\Omega, q_\perp, q_z) = N\left[\frac{q_\perp^2}{3\pi^2 v} \ln\left(\frac{\sqrt{A}\Lambda_{\mathrm{UV}}}{(\Omega^2 + A^2 q_\perp^4)^{1/4}} + 1 \right) + \frac{1}{64A} \frac{v q_z^2}{\sqrt{\Omega^2 + v^2 q_z^2}} \right] \qquad (13)$$

and

$$\Pi_t(i\Omega, q_\perp, q_z) = N\left[\frac{3q_\perp^2}{4\pi^2 v} \ln\left(\frac{B^{\frac{1}{3}}\Lambda_{\mathrm{UV}}}{(\Omega^2 + B^2 q_\perp^6)^{1/6}} + 1 \right) + c_t \frac{1}{B^{2/3}} \frac{v q_z^2}{(\Omega^2 + v^2 q_z^2)^{2/3}} \right], \qquad (14)$$

where c_t is a constant satisfying

$$c_t = \frac{2^{1/3}\pi^{1/2}}{90\Gamma(5/6)\Gamma(2/3)}. \qquad (15)$$

The Coulomb interaction remains long ranged because $\Pi_{d,t}(0, \mathbf{q})$ vanish in the limit $\mathbf{q} \to 0$.

III. RENORMALIZATION GROUP STUDY

To determine how model parameters flow with varying energy scale, we will employ the perturbative RG method [20,21,40,42,45,55–65]. Different from previous works on related topic [20,21,40,42], we will not adopt the instantaneous approximation and incorporate the dynamical screening of Coulomb interaction in our RG calculations.

A. Flow equations

The self-energy of double-Weyl fermions induced by the Coulomb interaction is formally given by

$$\Sigma_d(i\omega, \mathbf{k}) = \int' \frac{d\Omega}{2\pi} \frac{d^3\mathbf{q}}{(2\pi)^3} G_{d0}(i\omega + i\Omega, \mathbf{k} + \mathbf{q}) V_d(i\Omega, \mathbf{q}), \qquad (16)$$

where the notation $\int'$ implies that a momentum shell will be properly chosen in the calculation. Here, it is convenient to choose the momentum shell $b\Lambda < E_d(\mathbf{k}) < \Lambda$, where $b = e^{-\ell}$ with ℓ being a flow parameter. According to the calculations detailed in Appendix B 1, Σ_d can be approximated as

$$\Sigma_d(i\omega, \mathbf{k})$$
$$\approx \{i\omega C_{d1} - A[d_1(\mathbf{k})\sigma_x + d_2(\mathbf{k})\sigma_y]C_{d2} - vk_z\sigma_z C_{d3}\}\ell, \qquad (17)$$

to the leading order. The expressions of C_{d1}, C_{d2}, and C_{d3} are shown in Eqs. (B12)–(B15) in Appendix B 1.

According to the calculations of Appendix C 1, we find that the coupled RG equations are

$$\frac{dZ_f}{d\ell} = -C_{d1}Z_f, \qquad (18)$$

$$\frac{dA}{d\ell} = (C_{d2} - C_{d1})A, \qquad (19)$$

$$\frac{dv}{d\ell} = (C_{d3} - C_{d1})v, \qquad (20)$$

$$\frac{d\alpha}{d\ell} = (C_{d1} - C_{d3})\alpha, \qquad (21)$$

$$\frac{d\beta_d}{d\ell} = (C_{d1} + C_{d2} - 2C_{d3} - 1)\beta_d, \qquad (22)$$

$$\frac{d\gamma_d}{d\ell} = \frac{1}{2}(C_{d2} - C_{d1})\gamma_d. \qquad (23)$$

Here, the quasiparticle residue Z_f measures the overlap between free and interacting fermions, and $\alpha = e^2/v\epsilon$ characterizes the Coulomb interaction strength. The other two parameters are defined as

$$\beta_d = \frac{\zeta A \Lambda}{v^2}, \quad \gamma_d = \frac{\sqrt{A}\Lambda_{\mathrm{UV}}}{\sqrt{\Lambda}}. \qquad (24)$$

As shown in Appendix B 2, the self-energy of triple-Weyl fermions caused by Coulomb interaction can be written as

$$
\Sigma_t(i\omega, \mathbf{k}) = \int' \frac{d\Omega}{2\pi} \frac{d^3\mathbf{q}}{(2\pi)^3} G_{t0}(i\omega + i\Omega, \mathbf{k} + \mathbf{q}) V_t(i\Omega, \mathbf{q})
$$
$$
\approx \{i\omega C_{t1} - B[g_1(\mathbf{k})\sigma_x + g_2(\mathbf{k})\sigma_y]
$$
$$
\times C_{t2} - vk_z\sigma_z C_{t3}\}\ell. \tag{25}
$$

The momentum shell is taken as $b\Lambda < E_t(\mathbf{k}) < \Lambda$. The expressions of C_{t1}, C_{t2}, and C_{t3} are given by Eqs. (B27)–(B30) in Appendix B 2. As shown in Appendix C 2, the RG equations for triple-Weyl fermions are

$$
\frac{dZ_f}{d\ell} = -C_{t1}Z_f, \tag{26}
$$

$$
\frac{dB}{d\ell} = (C_{t2} - C_{t1})B, \tag{27}
$$

$$
\frac{dv}{d\ell} = (C_{t3} - C_{t1})v, \tag{28}
$$

$$
\frac{d\alpha}{d\ell} = (C_{t1} - C_{t3})\alpha, \tag{29}
$$

$$
\frac{d\beta_t}{d\ell} = \left(\frac{4}{3}C_{t1} + \frac{2}{3}C_{t2} - 2C_{t3} - \frac{4}{3}\right)\beta_t, \tag{30}
$$

$$
\frac{d\gamma_t}{d\ell} = \frac{1}{3}(C_{t2} - C_{t1})\gamma_t, \tag{31}
$$

where β_t and γ_t are defined as

$$
\beta_t = \frac{\zeta B^{2/3}\Lambda^{4/3}}{v^2}, \quad \gamma_t = \frac{B^{1/3}\Lambda_{\mathrm{UV}}}{\Lambda^{1/3}}. \tag{32}
$$

B. Quasiparticle residue and damping rate

The coupled flow equations can be solved numerically. The flow of quasiparticle residue $Z_f(\ell)$ for double-Weyl fermions is presented in Figs. 1(a)–1(c). According to Fig. 1(a), we find that $Z_f(\ell)$ eventually flows to zero in the limit $\ell \to \infty$, albeit at a small speed. Thus, the FL description is invalid, and the double-Weyl fermions are not well-defined Landau-type quasiparticles.

It is necessary to determine how rapidly $Z_f(\ell)$ vanishes. We observe from Fig. 1(b) that

$$
\lim_{\ell \to \infty} \frac{\ln(1/Z_f)}{\ell} \to 0. \tag{33}
$$

Based on Fig. 1(c), we find that $Z_f(\ell)$ exhibits the asymptotic behavior

$$
\lim_{\ell \to \infty} \frac{\ln(1/Z_f)}{\ln(\ell)} \to \eta, \tag{34}
$$

where η is a constant satisfying $0 < \eta < 1$. For physical flavor $N = 2$, $\eta \approx 0.18$. For large values of ℓ, $Z_f(\ell)$ behaves as

$$
Z_f(\ell) \sim \ell^{-\eta}. \tag{35}
$$

It is known that Z_f is connected to the real part of the retarded fermion self-energy $\mathrm{Re}\Sigma^R(\omega)$ via the relation

$$
Z_f(\omega) = \frac{1}{\left|1 - \frac{\partial}{\partial\omega}\mathrm{Re}\Sigma^R(\omega)\right|}. \tag{36}
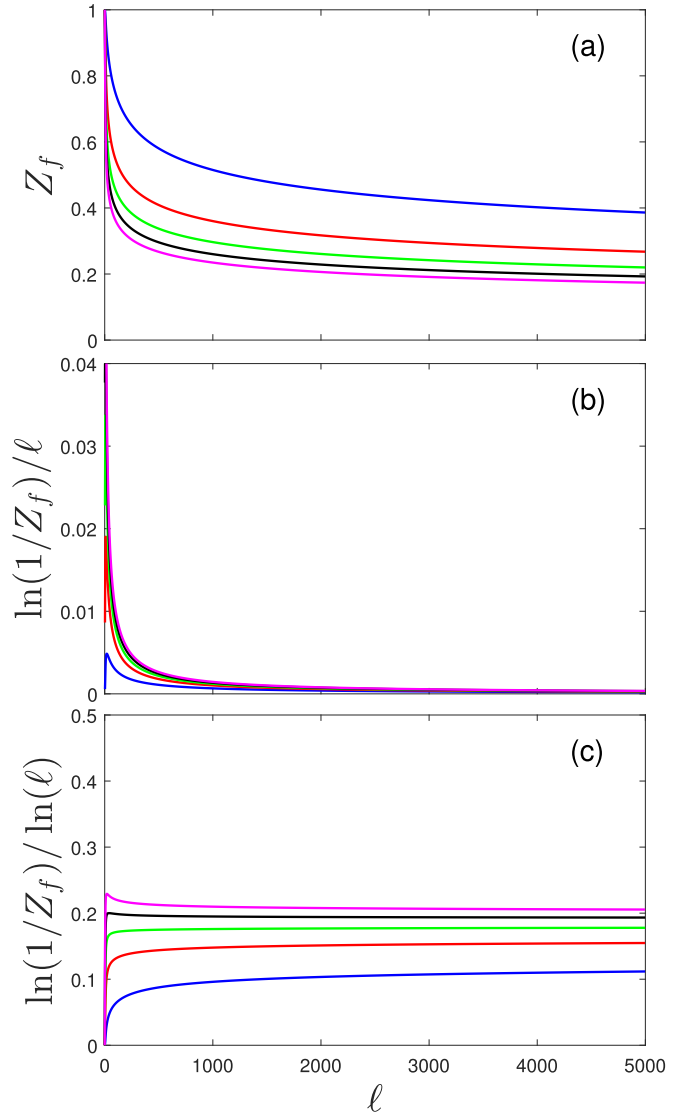$$

FIG. 1. Low-energy behavior of Z_f for double-Weyl fermions. The blue, red, green, black, and magenta lines correspond to $\alpha_0 = 0.1$, 0.5, 1, 1.5, and 2, respectively. $\beta_{d0} = 1$ and $\gamma_{d0} = 0.2$. Here, $N = 2$.

The ω dependence of Z_f can be obtained from $Z_f(\ell)$ by making the transformation $\omega = \omega_0 e^{-\ell}$, where ω_0 is some initial value of ω. On the basis of Eq. (36), it is now easy to obtain

$$
\mathrm{Re}\Sigma^R(\omega) \sim \omega\left[\ln\left(\frac{\omega_0}{\omega}\right)\right]^\eta. \tag{37}
$$

Employing the Kramers-Kronig relation [1], we get the imaginary part

$$
\mathrm{Im}\Sigma^R(\omega) \sim \frac{\omega}{[\ln(\omega_0/\omega)]^{1-\eta}}, \tag{38}
$$

which directly gives the fermion damping rate. The two equations (37) and (38) are the main results of this paper.

The asymptotic behavior of $Z_f(\ell)$ for triple-Weyl fermions can be similarly obtained by solving the flow equations. Results are shown in Figs. 2(a)–2(c). We find that $Z_f(\ell)$,
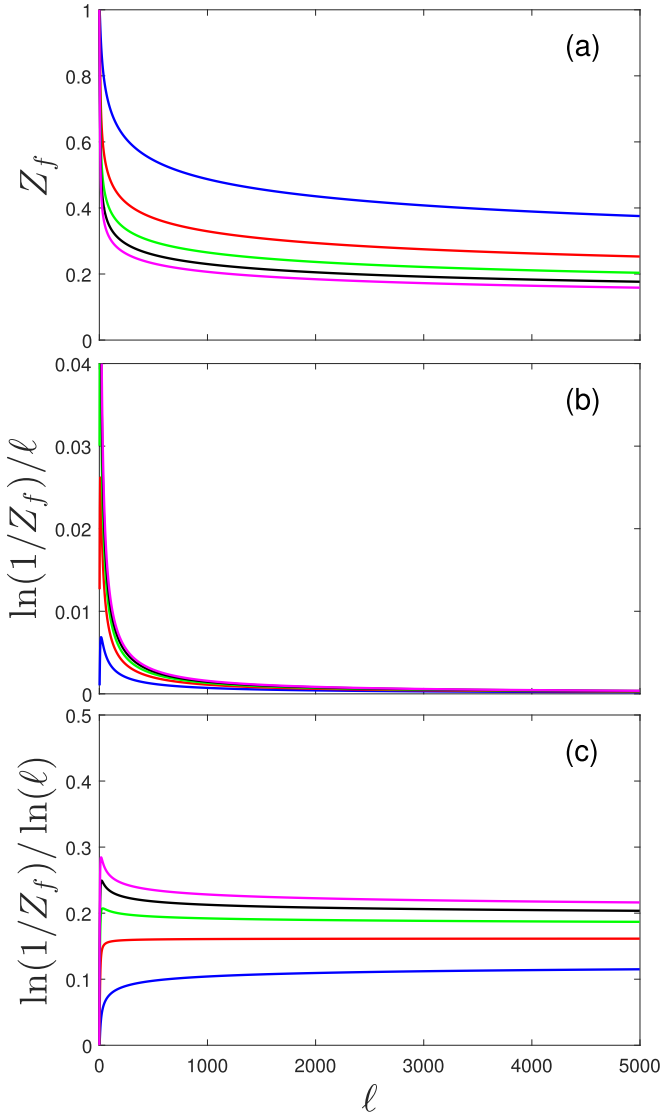
FIG. 2. Low-energy behavior of Z_f for triple-Weyl fermions. The blue, red, green, black, and magenta lines correspond to $\alpha_0 = 0.1, 0.5, 1, 1.5$, and 2, respectively. $\beta_{t0} = 1$, and $\gamma_{t0} = 0.2$. Here, $N = 2$.
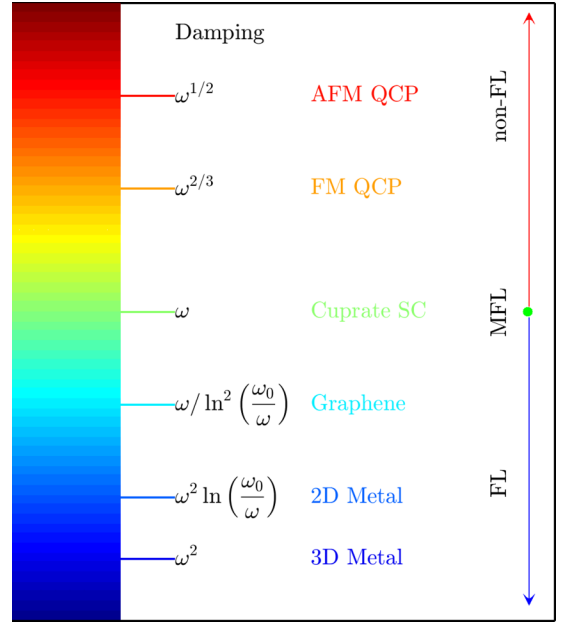

FIG. 3. Schematic illustration for traditional classification of FL, non-FL, and MFL. Interacting fermion system with damping rate weaker than MFL is believed to be a FL.

$\mathrm{Re}\Sigma^R(\omega)$, and $\mathrm{Im}\Sigma^R(\omega)$ exhibit almost the same qualitative low-energy behaviors as those of double-Weyl fermions, namely, they are also descried by Eqs. (35), (37), and (38). For $N = 2$, we find η can be also approximated by $\eta \approx 0.18$.

C. Fate of fermionic excitations in various interacting systems

To gain a better understanding of the uniqueness of the non-FL revealed in this work, we compare this state to a number of typical FLs and non-FLs, as summarized in Fig. 3. In many cases, the fermion damping rate can be expressed by a power law, i.e., $\mathrm{Im}\Sigma^R(\omega) \sim \omega^a$. One can verify that (i) for $0 < a < 1$, $Z_f \sim \omega^{1-a} \to 0$ as $\omega \to 0$; (ii) for $a = 1$, $Z_f \sim 1/\ln(\omega_0/\omega) \to 0$ as $\omega \to 0$; (iii) if $a > 1$, Z_f flows to a nonzero constant as $\omega \to 0$. An obvious conclusion is that FL theory is valid when $a > 1$, but breaks down when $0 < a \leqslant 1$. In 2D metal and graphene (2D DSM), the fermion damping rate is found to, respectively, depend on ω as $\omega^2 \ln(\omega_0/\omega)$ [1] and $\omega/\ln^2(\omega_0/\omega)$ [55], which are actually not power functions. However, the condition (1) is still satisfied in these two cases, and the corresponding residue $Z_f \neq 0$. Therefore, the condition (1) does provide an effective criterion to judge the validity of FL theory in all previously studied interacting fermion systems.

There is an interesting possibility that the damping rate vanishes at exactly the same speed as the energy, namely, $\Gamma(\omega) \sim \omega$. The residue Z_f decreases down to zero logarithmically as $\omega \to 0$. This behavior is broadly identified as the weakest violation of FL theory [4,12,14,15], which is the reason why an interacting fermion system displaying such a damping rate is called MFL. According to this notion, any system in which the Landau damping effect is weaker than MFL is usually regarded as a normal FL.

We emphasize here that, although the criterion (1) is widely utilized to judge the validity of FL theory in various interacting fermion systems, its efficiency has never been rigorously justified. There can be exceptions. It is in principle possible for Z_f to vanish more slowly than a logarithmic decrease. In this work, we demonstrate that this criterion breaks down in two concrete physical systems, namely, topological double- and triple-WSMs. Although the damping rate of multi-Weyl fermions satisfies the criterion (1), the residue Z_f vanishes in the limit $\omega \to 0$ more slowly than the logarithmic decrease. Thus, these two systems display a weaker-than-marginal violation of FL theory. An important indication of this result is that the FL theory could be spoiled even though the interparticle interaction does not induce a stronger-than-energy Landau damping. In this regard, the ground state of double- and triple-WSMs is distinct from all the other interacting fermion systems.

D. Comparing with usual Weyl semimetal

In this section, we study the residue and damping rate of fermions in usual WSM, and compare the results with double- and triple-WSMs. The free propagator of usual Weyl fermions is $G_{u0}^{-1}(i\omega, \mathbf{k}) = i\omega - v\mathbf{k} \cdot \sigma$. The dressed Coulomb interaction takes the form

$$V_u(i\Omega, \mathbf{q}) = \frac{1}{V_0^{-1}(\mathbf{q}) + \Pi_u(i\Omega, \mathbf{q})}, \qquad (39)$$

where $V_0(\mathbf{q}) = \frac{4\pi\alpha v}{|\mathbf{q}|^2}$, and the polarization is given by

$$\Pi_u(i\Omega, \mathbf{q})$$
$$= -N \int \frac{d\omega}{2\pi} \int \frac{d^3\mathbf{k}}{(2\pi)^3} \text{Tr}[G_{u0}(i\omega, \mathbf{k})G_{u0}(i\omega + i\Omega, \mathbf{k} + \mathbf{q})]$$
$$\approx \frac{N|\mathbf{q}|^2}{12\pi^2 v} \ln\left(\frac{v\Lambda_{\text{UV}} + \sqrt{\Omega^2 + v^2|\mathbf{q}|^2}}{\sqrt{\Omega^2 + v^2|\mathbf{q}|^2}}\right). \qquad (40)$$

Considering the self-energy induced by the Coulomb interaction

$$\Sigma_u(i\omega, \mathbf{k}) = \int' \frac{d\Omega}{2\pi} \frac{d^3\mathbf{q}}{(2\pi)^3} G_{u0}(i\omega + i\Omega, \mathbf{k} + \mathbf{q}) V_u(i\Omega, \mathbf{q})$$
$$\approx (i\omega C_{u1} - v\mathbf{k} \cdot \sigma C_{u2})\ell, \qquad (41)$$

and performing the RG analysis, we obtain the RG equations as follows:

$$\frac{dZ_f}{d\ell} = -C_{u1} Z_f, \qquad (42)$$

$$\frac{dv}{d\ell} = (C_{u2} - C_{u1})v, \qquad (43)$$

$$\frac{d\alpha}{d\ell} = (C_{u1} - C_{u2})\alpha, \qquad (44)$$

$$\frac{d\gamma_u}{d\ell} = (C_{u2} - C_{u1})\gamma_u, \qquad (45)$$

where

$$C_{u1} = \frac{1}{4\pi^3} \int_{-\infty}^{+\infty} dx \frac{x^2 - 1}{(x^2 + 1)^2} \mathcal{G}_u(x), \qquad (46)$$

$$C_{u2} = \frac{1}{4\pi^3} \int_{-\infty}^{+\infty} dx \frac{x^2 + \frac{1}{3}}{(x^2 + 1)^2} \mathcal{G}_u(x), \qquad (47)$$

with

$$\mathcal{G}_u^{-1}(x) = \frac{1}{4\pi\alpha} + \frac{N}{12\pi^2} \ln\left(\frac{\gamma_u e^\ell + \sqrt{x^2 + 1}}{\sqrt{x^2 + 1}}\right). \qquad (48)$$

The parameter γ_u is given by $\gamma_u = \frac{v\Lambda_{\text{UV}}}{\Lambda}$.

We have solved the above flow equations and plot the ℓ dependence of Z_f in Fig. 4. As ℓ grows, Z_f approaches to some finite value as $\ell \to \infty$. An immediate conclusion is that the unusual Weyl fermions are ordinary Landau-type quasiparticles, and the FL theory is well applicable. It is clear that usual WSM exhibits distinct behaviors than double- and triple-WSMs. The distinction originates from the difference in the fermion dispersion.
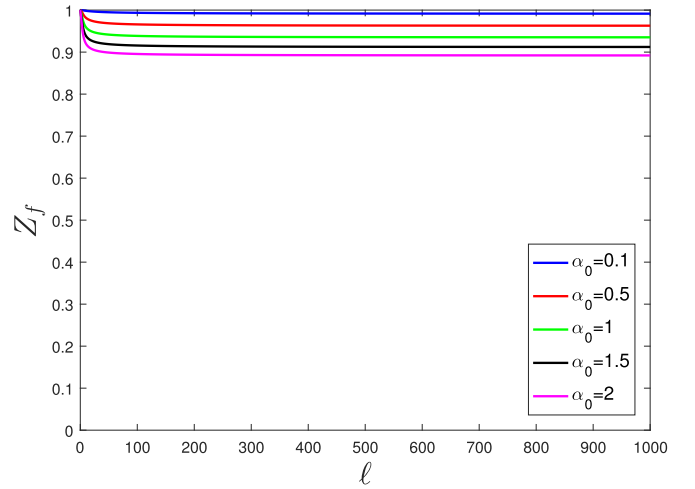

FIG. 4. The residue Z_f of interacting usual Weyl fermions flows to certain finite constant as $\ell \to \infty$. Therefore, the Coulomb interaction does not violate the FL theory.

IV. OBSERVABLE QUANTITIES

As demonstrated in the last section, the non-FL state of double- and triple-WSMs is qualitatively different from normal FLs and conventional non-FLs. In this section, we discuss the possible experimental signatures of this state. The residue Z_f is not directly measurable. Here, we will compute a number of observable quantities, including the spectral function, DOS, specific heat, and conductivities, and analyze their low-energy properties. The calculational details can be found in Appendices E and F.

A. Spectral function

We first consider the fermion spectral function $\mathcal{A}(\omega, \mathbf{k})$ and the damping rate $\Gamma(\omega)$. In the noninteracting limit, the spectral function is just a δ function, namely,

$$\mathcal{A}_0(\omega, \mathbf{k}) = \delta(\omega - \xi_\mathbf{k}),$$

where $\xi_\mathbf{k}$ is the kinetic energy, which displays an infinitely sharp peak. After including quantum many-body effects, it becomes

$$\mathcal{A}(\omega, \mathbf{k}) = \frac{1}{\pi} \frac{|\text{Im}\Sigma^R(\omega)|}{[\omega + \text{Re}\Sigma^R(\omega) - \xi_\mathbf{k}]^2 + [\text{Im}\Sigma^R(\omega)]^2}. \qquad (49)$$

In Fig. 5, we list four different cases: 3D metal as a normal FL; unconventional non-FL state revealed in this paper; MFL; conventional non-FL. As shown in Fig. 5(a), the energy distribution curve (EDC) for 3D metal has a very sharp peak. Around an AFM QCP, depicted in Fig. 5(f), the EDC exhibits an obviously asymmetric shape with a long tail. We observe from Fig. 5(e) that the EDC of MFL still displays a weak asymmetry. For the unusual non-FL states demonstrated in Figs. 5(b)–5(d), the asymmetry of EDC is even weaker than that of MFL, and the asymmetry is gradually weakened as η decreases. Nevertheless, the peak width is larger than that of normal FLs, which is consistent with the fact that $Z_f = 0$. Comparing the EDCs shown in Figs. 5(a)–5(f), we can infer that the non-FL state realized in double- and triple-WSMs stays in-between MFL and all the normal FLs. ARPES
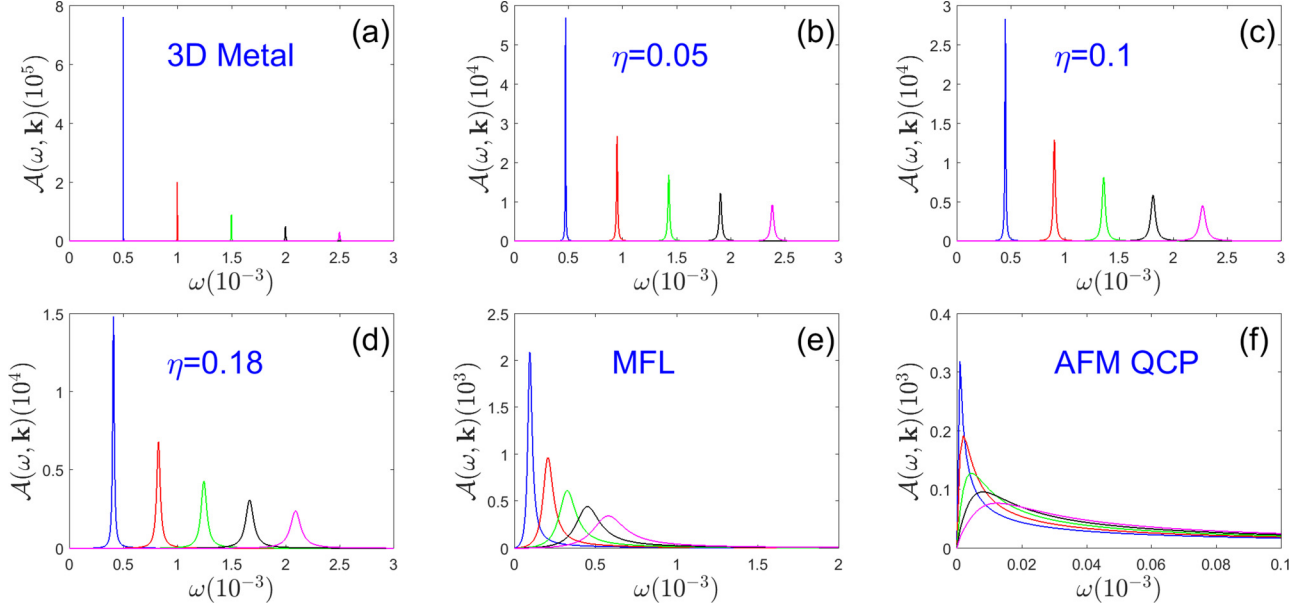
FIG. 5. Energy distribution curves in a number of FLs and non-FLs. (a) 3D metal; (b)–(d) unconventional non-FL with $\eta = 0.18$ corresponding to physical flavor $N = 2$; (e) MFL; (f) non-FL realized at an AFM QCP. The blue, red, green, black, and magenta curves correspond to $\xi_{\mathbf{k}} = 0.001$, 0.002, 0.003, 0.004, and 0.005, respectively.

experiments [46–54] could be performed to detect the peculiar properties of EDCs of the unconventional non-FL state.

The fermion damping rate $\Gamma(\omega)$ can be extracted from the ARPES data of EDC or momentum distribution curve (MDC) [46,47]. It is especially efficient to fit MDC with the Lorentzian peak [46–53]. High-resolution ARPES measurements have been extensively applied to determine the fermion damping rate in many correlated electron systems, including cuprates [46–48], iron pnictides [49,50], graphene [51], and topological insulators [52,53]. We expect that the unconventional damping rate, i.e., $\Gamma(\omega) \sim \omega/[\ln(\omega_0/\omega)]^{1-\eta}$, obtained in our work could be investigated by using this experimental tool in the future.

B. DOS

The DOS of free double-Weyl fermions is linear in energy, i.e.,

$$\rho_d(\omega) = \frac{N}{8\pi v A}|\omega|.\tag{50}$$

The Coulomb interaction leads to singular renormalization of the parameters A and v. The flows of A and v can be obtained from the RG equations, with results shown in Figs. 6(a) and 6(b). Both A and v increase as ℓ is growing, and it is obvious that A increases more rapidly than v. After incorporating the anomalous dimension of fermion field and the renormalization of A and v, we get the following RG equation for ρ_d:

$$\frac{d\ln(\rho_d(\omega))}{d\ln(\omega)} \sim 1 - C_{d1} + C_{d2} + C_{d3}.\tag{51}$$

As depicted in Fig. 7(a), the double-Weyl fermion DOS is suppressed by Coulomb interaction.

For free triple-Weyl fermions, the DOS is given by

$$\rho_t(\omega) = \frac{N\Gamma(1/3)}{12\pi^{3/2}\Gamma(5/6)vB^{2/3}}|\omega|^{2/3}.\tag{52}$$

The ℓ dependence of B and v is plotted in Figs. 6(c) and 6(d). Both B and v increase with growing ℓ, but at different speeds. Including the interaction corrections modifies $\rho_t(\omega)$, and yields

$$\frac{d\ln(\rho_t(\omega))}{d\ln(\omega)} \sim \frac{2}{3} - \frac{2}{3}C_{t1} + \frac{2}{3}C_{t2} + C_{t3}.\tag{53}$$

The energy dependence of $\rho_t(\omega)$ is depicted in Fig. 7(c). The DOS of triple-Weyl fermions is also suppressed by the Coulomb interaction.
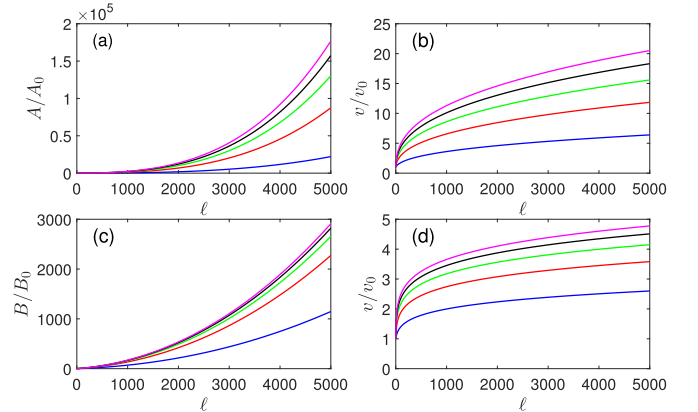

FIG. 6. (a), (b) Flows of A and v in double-WSM with $\beta_{d0} = 1$, $\gamma_{d0} = 0.2$, and $N = 2$. (c), (d) Flows of B and v in triple-WSM with $\beta_{t0} = 1$, $\gamma_{t0} = 0.2$, and $N = 2$. In (a)–(d), blue, red, green, black, and magenta lines correspond to $\alpha_0 = 0.1, 0.5, 1, 1.5$, and 2, respectively.
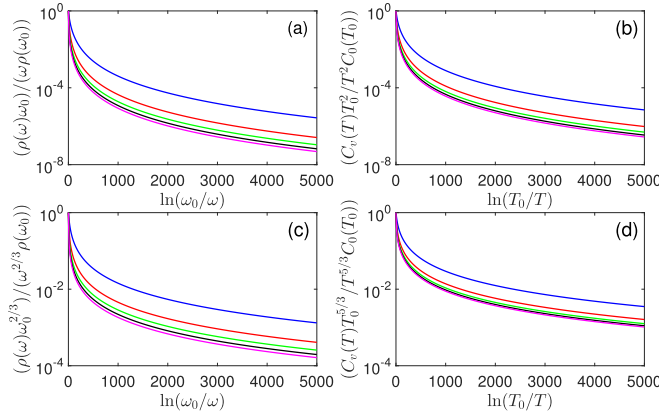
FIG. 7. DOS and specific heat of double- and triple-WSMs after including the Coulomb interaction corrections. (a), (b) Results for double-WSM with $\beta_{d0} = 1$, $\gamma_{d0} = 0.2$, and $N = 2$. (c), (d) Results for triple-WSM with $\beta_{t0} = 1$, $\gamma_{t0} = 0.2$, and $N = 2$. In (a)–(d), blue, red, green, black, and magenta lines correspond to $\alpha_0 = 0.1, 0.5, 1, 1.5$, and 2, respectively.

C. Specific heat

The specific heat for free double- and triple-Weyl fermions is

$$C_v^d(T) = \frac{9\zeta(3)N}{4\pi v A} T^2, \tag{54}$$

$$C_v^t(T) = \frac{40 a_t N}{9\pi^{3/2} v B^{2/3}} T^{5/3}, \tag{55}$$

respectively. Here, a_t is a constant. Taking into account the renormalization of parameters A, B, and v, we derive the following equations:

$$\frac{d \ln \left(C_v^d(T) \right)}{d \ln(T)} \sim 2 - 2C_{d1} + C_{d2} + C_{d3}, \tag{56}$$

$$\frac{d \ln \left(C_v^t(T) \right)}{d \ln(T)} \sim \frac{5}{3} - \frac{5}{3}C_{t1} + \frac{2}{3}C_{t2} + C_{t3}. \tag{57}$$

The corresponding numerical results are presented in Figs. 7(b) and 7(d). It is clear that the specific heat is suppressed by the Coulomb interaction in both systems.

D. Conductivities

Transport properties might provide important information on the experimental signatures of non-FL state. Here, we are particularly interested in the conductivities. We will first estimate the dc conductivities, and then calculate the dynamical conductivities.

1. Estimation of dc conductivities

To estimate the dc conductivity, a heuristic method is to invoke the Einstein relation [1,2,58,66]

$$\sigma \sim e^2 v^2 \rho(E) \tau(E), \tag{58}$$

where v is the mean fermion velocity, ρ the DOS, and τ the mean fermion lifetime. E stands for either energy or

temperature. Since τ is inversely proportional to the damping rate Γ, i.e.,

$$\tau \sim \frac{1}{\Gamma}, \tag{59}$$

the Einstein relation can be rewritten as

$$\sigma \sim e^2 v^2 \rho(E)/\Gamma(E). \tag{60}$$

In conventional metals, the fermion damping rate is $\Gamma(E) \sim E^2$ [1,2], whereas v and ρ are both constants in the low-energy regime. Taking $E = T$, one can easily obtain

$$\sigma \sim T^{-2}. \tag{61}$$

This indicates that the resistivity

$$R \sim \frac{1}{\sigma} \sim T^2, \tag{62}$$

which is a well-known characteristic of conventional metals [1,2]. We will utilize this procedure to estimate the dc conductivities of double- and triple-WSMs.

For double-WSM, the DOS is given by $\rho(E) \sim E/(vA)$. The damping rate is $\Gamma(E) \sim E/[\ln(E_0/E)]^{1-\eta}$, which can be further simplified to $\Gamma(E) \sim E$ if the weak logarithmiclike factor is neglected. The fermion velocity within the x-y plane takes the form

$$v_\perp \sim A k_\perp \sim \sqrt{AE}. \tag{63}$$

By using the Einstein relation, we find that the conductivity within the x-y plane can be approximately expressed as

$$\sigma_{\perp\perp}^d(T) \sim T. \tag{64}$$

The fermion velocity along the z axis is v, thus the corresponding conductivity is independent of T, namely,

$$\sigma_{zz}^d(T) \sim T^0 \sim \text{const}. \tag{65}$$

For triple-WSM, the DOS depends on energy in the form $\rho(E) \sim E^{2/3}/(vB^{2/3})$. The damping rate behaves as $\Gamma(E) \sim E/(\ln(E_0/E))^{1-\eta}$, which is approximated by $\Gamma(E) \sim E$. The fermion velocity within the x-y plane reads as

$$v_\perp \sim B k_\perp^2 \sim B^{1/3} E^{2/3}. \tag{66}$$

Employing the Einstein relation, we obtain the conductivity within the x-y plane

$$\sigma_{\perp\perp}^t(T) \sim T, \tag{67}$$

which is qualitatively the same as the one for double-WSM. However, different from double-WSM, the conductivity along z axis is T dependent, given by

$$\sigma_{zz}^t(T) \sim T^{-1/3}. \tag{68}$$

In the above estimation, we neglect the weak logarithmiclike factor that exists in the damping rate and the renormalized parameters (A, B, and v). If these corrections are incorporated, the conductivities could receive weak logarithmiclike corrections in their temperature dependence.

2. Dynamical conductivities

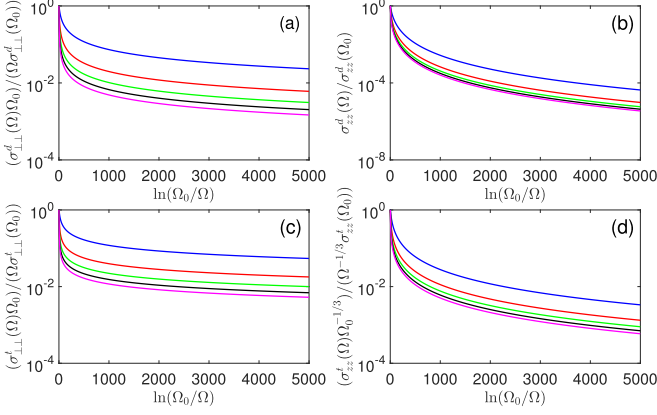We next analyze the properties of dynamical conductivities by including the energy dependence. By using the Kubo

FIG. 8. Dynamical conductivities of double- and triple-WSMs considering the influence of Coulomb interaction. (a), (b) $\sigma_{\perp\perp}^d$ and σ_{zz}^d for double-WSM with $\beta_{d0} = 1$, $\gamma_{d0} = 0.2$, and $N = 2$. (c), (d) $\sigma_{\perp\perp}^t$ and σ_{zz}^t for triple-WSM with $\beta_{t0} = 1$, $\gamma_{t0} = 0.2$, and $N = 2$. In (a)–(d), blue, red, green, black, and magenta lines correspond to $\alpha_0 = 0.1, 0.5, 1, 1.5$, and 2, respectively.

formula, we get the dynamical conductivities for free double-Weyl fermions within the x-y plane and along the z axis:

$$\sigma_{\perp\perp}^d(\Omega, T) = c_1^d \frac{e^2}{v} \delta(\Omega) T^2 + c_2^d \frac{e^2}{v} |\Omega| \tanh\left(\frac{|\Omega|}{4T}\right), \quad (69)$$

$$\sigma_{zz}^d(\Omega, T) = c_3^d \frac{ve^2}{A} \delta(\Omega) T + c_4^d \frac{ve^2}{A} \tanh\left(\frac{|\Omega|}{4T}\right). \quad (70)$$

The constants c_1^d, c_2^d, c_3^d, and c_4^d are given in Appendix E 2 a. The first terms on the right-hand sides of Eqs. (69) and (70) indicate the presence of Drude peak. At zero temperature, the dynamical conductivities become

$$\sigma_{\perp\perp}^d(\Omega) = c_2^d \frac{e^2}{v} |\Omega|, \quad (71)$$

$$\sigma_{zz}^d(\Omega) = c_4^d \frac{ve^2}{A}. \quad (72)$$

Incorporating the interaction corrections, we derive the RG equations for $\sigma_{\perp\perp}^d$ and σ_{zz}^d:

$$\frac{d \ln\left(\sigma_{\perp\perp}^d(\Omega)\right)}{d \ln(\Omega)} \sim 1 + C_{d1} + C_{d3}, \quad (73)$$

$$\frac{d \ln\left(\sigma_{zz}^d(\Omega)\right)}{d \ln(\Omega)} \sim 2C_{d1} + C_{d2} - C_{d3}. \quad (74)$$

The solutions of these two equations are shown in Figs. 8(a) and 8(b). Both $\sigma_{\perp\perp}^d$ and σ_{zz}^d are suppressed by the Coulomb interaction.

For free triple-Weyl fermions, the dynamical conductivities within the x-y plane and along the z axis are

$$\sigma_{\perp\perp}^t(\Omega, T) = c_1^t \frac{e^2}{v} \delta(\Omega) T^2 + c_2^t \frac{e^2}{v} |\Omega| \tanh\left(\frac{|\Omega|}{4T}\right), \quad (75)$$

$$\sigma_{zz}^t(\Omega, T) = c_3^t \frac{ve^2}{B^{2/3}} \delta(\Omega) T^{2/3} + c_4^t \frac{ve^2}{B^{2/3}} \frac{1}{|\Omega|^{1/3}} \tanh\left(\frac{|\Omega|}{4T}\right). \quad (76)$$

The constants c_1^t, c_2^t, c_3^t, and c_4^t are shown in Appendix E 2 b. At zero temperature, they behave as

$$\sigma_{\perp\perp}^t(\Omega) = c_2^t \frac{e^2}{v} |\Omega|, \quad (77)$$

$$\sigma_{zz}^t(\Omega) = c_4^t \frac{ve^2}{B^{2/3}} \frac{1}{|\Omega|^{1/3}}. \quad (78)$$

The Coulomb interaction alters the above behaviors and gives rise to the following equations:

$$\frac{d \ln(\sigma_{\perp\perp}^t(\Omega))}{d \ln(\Omega)} \sim 1 + C_{t1} + C_{t3}, \quad (79)$$

$$\frac{d \ln\left(\sigma_{zz}^t(\Omega)\right)}{d \ln(\Omega)} \sim -\frac{1}{3} + \frac{7}{3}C_{t1} + \frac{2}{3}C_{t2} - C_{t3}. \quad (80)$$

The detailed energy dependence of $\sigma_{\perp\perp}^t$ and σ_{zz}^t can be found from Figs. 8(c) and 8(d).

V. EXPERIMENTAL DETECTION

It was recently suggested that $HgCr_2Se_4$ [19] and $SrSi_2$ [67] are two candidate materials of double-WSM. Theoretical studies [68] proposed that cubic-Dirac SM (cubic-DSM), in which the fermion dispersion is linear in one momentum component and cubic in the rest two, might be realized in some materials, including $Rb(MoTe)_3$ and $Tl(MoTe)_3$ that belong to the $A(MoX)_3$ family. Similar to triple-WSM, such cubic-DSMs should also display the unconventional non-FL behavior. The physical fermion flavor is $N = 2$ in $HgCr_2Se_4$ [19], thus $\eta \approx 0.18$. In $SrSi_2$, the flavor of double-Weyl fermions is $N = 8$ [67], for which we get $\eta \approx 0.05$. In $Rb(MoTe)_3$ and $Tl(MoTe)_3$, there is only one type of cubic Dirac fermion, formed by the degeneracy of two species of triple-Weyl fermions [68]. Accordingly, we find that $\eta \approx 0.18$ in these two materials.

The unconventional non-FL state is induced by the long-range Coulomb interaction, thus, its signature is sharpest at zero chemical potential, i.e., $\mu = 0$, which can be realized by tuning the Fermi level to the band-touching point. In real materials, μ is usually not strictly zero, but takes a finite value. For finite μ, the Coulomb interaction becomes short ranged due to the static screening caused by finite zero-energy DOS. It is necessary to emphasize that the unconventional non-FL state still has observable effects at finite μ. At energies below μ, namely, $\omega < \mu$, the system exhibits ordinary FL behavior. At energies above μ, namely, $\omega > \mu$, the static screening becomes relatively unimportant, and non-FL behavior reemerges. As ω further grows, the Coulomb interaction might be surpassed by other interactions, such as electron-phonon coupling. Thus, non-FL behavior actually occurs in a finite range of intermediate energies $\mu < \omega < \omega_c$, where ω_c is a material-dependent upper energy scale. This energy range narrows when μ increases, and finally disappears once μ becomes large enough. For sufficiently small μ, there are always observable signatures of the unconventional non-FL state. To intuitively understand what happens at finite μ, one could regard μ as a tuning parameter: $\mu = 0$ defines a special QCP that exhibits an unconventional non-FL ground state
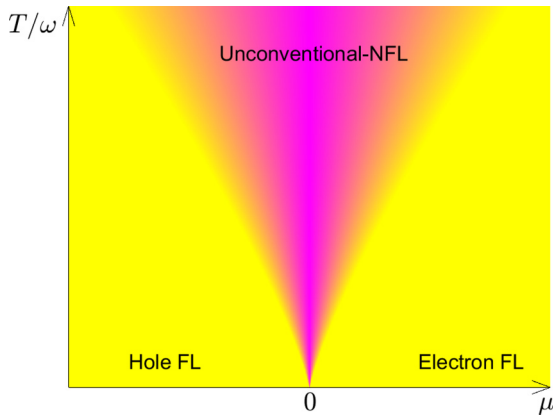
FIG. 9. Phase diagram for multi-WSM in the parameter space spanned by μ and T/ω. The unconventional non-FL state can be probed in the whole quantum critical regime.

at lowest-energy limit. This QCP is broadened into a finite quantum critical regime at finite T/ω, as schematically shown in Fig. 9. Unconventional non-FL behavior emerges in this regime, and can be explored at finite T with $T > \mu$ or at finite ω with $\omega > \mu$.

It is technically possible to reduce μ gradually, by either doping manipulation or gate voltage control [51,69–74]. Some unusual quantum many-body effects have already been observed in SM samples prepared at small μ [51,69–72,75]. For instance, RG studies predicted that the fermion velocity is singularly renormalized by long-range Coulomb interaction in 2D DSM [55,56]. This prediction was recently confirmed in graphene with small μ by a number of different experimental tools, including ARPES [51], Shubnikov–de Haas oscillations [69], scanning tunneling spectroscopy [70], quantum capacitance measurements [71], and Landau level spectroscopy [75].

Remarkably, one could fix the Fermi level of SM at exactly the band-touching point via the mechanism of symmetry protection [16,76–79], which naturally realizes ideal SM with $\mu = 0$. Such symmetry-protected ideal WSM state is proposed to exist in several materials, including strained HgTe and Heusler compounds [76], some chalcopyrite compounds [77], GdSI [78], and CuF [79]. If symmetry-protected ideal double- and triple-WSMs were discovered in the future, it would be more feasible to probe the unconventional non-FL behavior.

VI. SUMMARY

In summary, we have studied two important quantities, the quasiparticle residue and the Landau damping rate, in double- and triple-WSMs. The result is that the residue Z_f flows to zero in the lowest-energy limit, but at a lower speed than that of the MFL. Based on the energy dependence of Z_f, we have obtained the real and imaginary parts of the retarded fermion self-energy, and then computed the spectral function. Interestingly, the Landau damping rate is weaker than the one of MFL. These results imply that the Coulomb interaction leads to a weaker-than-marginal breakdown of the FL theory in both double- and triple-WSMs. The unconventional non-FL state can be experimentally probed by measuring the fermion

self-energy and the spectral function. We have also calculated several other observable quantities, including DOS, specific heat, and conductivities, and discussed the impact of the anomalous interaction corrections. We would emphasize that this non-FL state has observable effects even at finite chemical potential.

Notice that the Coulomb interaction is long ranged in all the DSMs and WSMs that host isolated band-touching points. However, this new type of non-FL state emerges only in double- and triple-WSMs, but has never been found neither in the 2D/3D DSMs nor in the usual WSMs. In order to make a comparison between different types of WSMs, we have computed the residue Z_f of usual Weyl fermions and found that it flows to a finite value as the energy is lowered down to zero. The difference indicates that the influence of long-range Coulomb interaction in SMs is closely linked to the energy dispersion of the fermion excitations.

The impact of Coulomb interaction has recently been studied in double-WSM [20,21] and triple-WSM [40,42] by means of the RG method. These RG studies are based on the instantaneous approximation (neglecting the energy dependence of Coulomb interaction), and thus do not provide any information about the residue Z_f and fermion damping rate $\Gamma(\omega)$. Different from Refs. [20,21,40,42], we have incorporated the dynamical screening of Coulomb interaction in our RG analysis and obtained both the residue and damping rate.

APPENDIX A: CALCULATION OF POLARIZATION FUNCTIONS

Although the Coulomb interaction is long ranged at zero chemical potential, it is dynamically screened by the collective particle-hole excitations. The dynamical screening effect is embodied in the energy/momentum dependence of the polarization functions. The aim of this appendix is to calculate the polarizations $\Pi_{d,t}(\Omega, \mathbf{q})$ for double- and triple-Weyl fermions.

1. Polarization $\Pi_d(\Omega, \mathbf{q})$ of double-Weyl fermions

For double-Weyl fermions, the polarization is given by

$$\Pi_d(i\Omega, \mathbf{q}) = -N \int \frac{d\omega}{2\pi} \int \frac{d^3\mathbf{k}}{(2\pi)^3} \text{Tr}[G_{d0}(i\omega, \mathbf{k})$$
$$\times G_{d0}(i\omega + i\Omega, \mathbf{k} + \mathbf{q})]. \quad \text{(A1)}$$

Substituting the fermion propagator (7) into Eq. (A1), we get

$$\Pi_d\left(i\Omega, \frac{q_x}{\sqrt{A}}, \frac{q_y}{\sqrt{A}}, \frac{q_z}{v}\right) = \frac{2N}{Av} \int \frac{d\omega}{2\pi} \int \frac{d^3\mathbf{k}}{(2\pi)^3} \frac{F_{d1}^A}{F_{d1}^B}, \quad \text{(A2)}$$

where

$$F_{d1}^A = \omega(\omega + \Omega) - \sum_{i=1}^{3} d_i(\mathbf{k}) d_i(\mathbf{k} + \mathbf{q}), \quad (A3)$$

$$F_{d1}^B = (\omega^2 + E_{\mathbf{k}}^2)[(\omega + \Omega)^2 + E_{\mathbf{k}+\mathbf{q}}^2], \quad (A4)$$

with $d_1(\mathbf{k}) = k_x^2 - k_y^2$, $d_2(\mathbf{k}) = 2k_x k_y$, $d_3(\mathbf{k}) = k_z$, and $E_{\mathbf{k}} = \sqrt{k_\perp^4 + k_z^2}$. This expression is obtained by making the following rescaling transformations:

$$k_x \to \frac{k_x}{\sqrt{A}}, \quad q_x \to \frac{q_x}{\sqrt{A}}, \quad k_y \to \frac{k_y}{\sqrt{A}},$$
$$q_y \to \frac{q_y}{\sqrt{A}}, \quad k_z \to \frac{k_z}{v}, \quad q_z \to \frac{q_z}{v}. \quad (A5)$$

Employing the Feynman integral

$$\frac{1}{XY} = \int_0^1 dx \frac{1}{[xX + (1-x)Y]^2}, \quad (A6)$$

the polarization can be further written as

$$\Pi_d\left(i\Omega, \frac{q_x}{\sqrt{A}}, \frac{q_y}{\sqrt{A}}, \frac{q_z}{v}\right)$$
$$= \frac{2N}{Av} \int_0^1 dx \int \frac{dk_x \, dk_y}{2\pi \, 2\pi} F_{d2}^A \int \frac{d^2\mathbf{K}}{(2\pi)^2} \frac{1}{(F_{d2}^B)^2}, \quad (A7)$$

where

$$F_{d2}^A = -x(1-x)(\Omega^2 - q_z^2) - d_1\left(\mathbf{k} - \frac{\mathbf{q}}{2}\right) d_1\left(\mathbf{k} + \frac{\mathbf{q}}{2}\right)$$
$$- d_2\left(\mathbf{k} - \frac{\mathbf{q}}{2}\right) d_2\left(\mathbf{k} + \frac{\mathbf{q}}{2}\right), \quad (A8)$$

$$F_{d2}^B = K^2 + x(1-x)(\Omega^2 + q_z^2) + (1-x)\left(\mathbf{k} - \frac{\mathbf{q}}{2}\right)_\perp^4$$
$$+ x\left(\mathbf{k} + \frac{\mathbf{q}}{2}\right)_\perp^4, \quad (A9)$$

and $\mathbf{K} = (\omega, k_z)$. The transformations $k_x \to k_x - \frac{q_x}{2}$ and $k_y \to k_y - \frac{q_y}{2}$ have been made in the above derivation. We then integrate over $\mathbf{K}$ by using the formula

$$\int \frac{d^d Q}{(2\pi)^d} \frac{1}{(Q^2 + \Delta)^n} = \frac{\Gamma(n - d/2)}{(4\pi)^{d/2} \Gamma(n)} \frac{1}{\Delta^{n-d/2}}, \quad (A10)$$

and obtain

$$\Pi_d\left(i\Omega, \frac{q_x}{\sqrt{A}}, \frac{q_y}{\sqrt{A}}, \frac{q_z}{v}\right)$$
$$= \frac{N}{2\pi A v} \int_0^1 dx \int \frac{dk_x \, dk_y}{2\pi \, 2\pi} \left(\frac{F_{d3}^A}{F_{d3}^B} + 1\right), \quad (A11)$$

where

$$F_{d3}^A = -x(1-x)(\Omega^2 - q_z^2) - \left(k_\perp^2 - \frac{q_\perp^2}{4}\right)^2$$
$$+ (k_y q_x - k_x q_y)^2, \quad (A12)$$

$$F_{d3}^B = x(1-x)(\Omega^2 + q_z^2) + \left(k_\perp^2 + \frac{q_\perp^2}{4}\right)^2 + (k_x q_x + k_y q_y)^2$$
$$- 2(1-2x)\left(k_\perp^2 + \frac{q_\perp^2}{4}\right)(k_x q_x + k_y q_y). \quad (A13)$$

This polarization has already been regularized by replacing $\Pi_d(i\Omega, \frac{q_x}{\sqrt{A}}, \frac{q_y}{\sqrt{A}}, \frac{q_z}{v})$ with $\Pi_d(i\Omega, \frac{q_x}{\sqrt{A}}, \frac{q_y}{\sqrt{A}}, \frac{q_z}{v}) - \Pi_d(0, 0, 0, 0)$. We now introduce the polar coordinates, and rewrite the polarization as

$$\Pi_d\left(i\Omega, \frac{q_\perp}{\sqrt{A}}, q_z\right) = \frac{N}{8\pi^3 A v} \int_0^1 dx \int_0^{\Lambda_{\mathrm{UV}}} dk_\perp k_\perp$$
$$\times \int_0^{2\pi} d\theta \left(\frac{F_{d4}^A}{F_{d4}^B} + 1\right), \quad (A14)$$

where

$$F_{d4}^A = -x(1-x)(\Omega^2 - q_z^2) - \left(k_\perp^2 - \frac{q_\perp^2}{4}\right)^2 + k_\perp^2 q_\perp^2 \sin^2(\theta), \quad (A15)$$

$$F_{d4}^B = x(1-x)(\Omega^2 + q_z^2) + \left(k_\perp^2 + \frac{q_\perp^2}{4}\right)^2 + k_\perp^2 q_\perp^2 \cos^2(\theta)$$
$$- 2(1-2x)\left(k_\perp^2 + \frac{q_\perp^2}{4}\right) k_\perp q_\perp \cos(\theta). \quad (A16)$$

θ is the angle between $\mathbf{k}_\perp$ and $\mathbf{q}_\perp$, and Λ_{UV} is an UV cutoff. This polarization is formally very complicated, and cannot be directly used to calculate fermion self-energy. To proceed, we will analyze its asymptotic behaviors in several different limits, and then obtain an appropriate approximate expression. This strategy is widely employed in the study of interacting fermion systems [1,2,4,64].

a. $q_\perp = 0$

In the limit $q_\perp = 0$, the polarization takes the form

$$\Pi_d\left(i\Omega, 0, \frac{q_z}{v}\right) = \frac{N}{2\pi^2 A v} q_z^2 \int_0^1 dx \, x(1-x)$$
$$\times \int_0^{\Lambda_{\mathrm{UV}}} dk_\perp k_\perp \frac{1}{x(1-x)(\Omega^2 + q_z^2) + k_\perp^4}. \quad (A17)$$

The upper limit of the integration over $k_\perp$ can be taken to be infinity, which leads to

$$\Pi_d\left(i\Omega, 0, \frac{q_z}{v}\right) = \frac{N}{64 A v} \frac{q_z^2}{\sqrt{\Omega^2 + q_z^2}}. \quad (A18)$$

b. $\Omega = 0$ and $q_z = 0$

Setting $\Omega = 0$ and $q_z = 0$, integrating over x, and then making the transformation $k_\perp = q_\perp y$, we obtain

$$\Pi_d\left(0, \frac{q_\perp}{\sqrt{A}}, 0\right) = \frac{N q_\perp^2}{8\pi^3 A v} \int_0^{\frac{\pi}{2}} d\theta \int_0^{\frac{\Lambda_{\mathrm{UV}}}{q_\perp}} dy \, F_{d5}, \quad (A19)$$

where

$$F_{d5} = 4y + 2\frac{y^2\sin^2(\theta) - \left(y^2 - \frac{1}{4}\right)^2}{\left(y^2 + \frac{1}{4}\right)\cos(\theta)}$$
$$\times \ln\left(\frac{y^2 + \frac{1}{4} + y\cos(\theta)}{y^2 + \frac{1}{4} - y\cos(\theta)}\right). \tag{A20}$$

In the limit $y \to \infty$, it is easy to verify that

$$F_{d5} \to \frac{16 - 8\cos(2\theta)}{3y}. \tag{A21}$$

In the low-energy regime, $\Pi(0, \frac{q_\perp}{\sqrt{A}}, 0)$ is given by

$$\Pi_d\left(0, \frac{q_\perp}{\sqrt{A}}, 0\right) \approx \frac{Nq_\perp^2}{8\pi^3 Av}\left[a_1 + a_2 + \frac{8\pi}{3}\ln\left(\frac{\Lambda_{\rm UV}}{q_\perp}\right)\right], \tag{A22}$$

where

$$a_1 = \int_0^{\frac{\pi}{2}} d\theta \int_0^1 dy\, F_{d5}, \tag{A23}$$

$$a_2 = \int_0^{\frac{\pi}{2}} d\theta \int_1^{+\infty} dy\left[F_{d5} - \frac{16 - 8\cos(2\theta)}{3y}\right]. \tag{A24}$$

Through numerical calculation, we find that

$$a_1 \approx 3.835\,04, \quad a_2 \approx -1.4367. \tag{A25}$$

Retaining the leading contribution yields

$$\Pi_d\left(0, \frac{q_\perp}{\sqrt{A}}, 0\right) = \frac{Nq_\perp^2}{3\pi^2 Av}\ln\left(\frac{\Lambda_{\rm UV}}{q_\perp}\right). \tag{A26}$$

c. $q_z = 0$ and $q_\perp^2 \ll \Omega$

In the limit $q_z = 0$ and $q_\perp^2 \ll \Omega$, the polarization can be approximated by

$$\Pi_d\left(i\Omega, \frac{q_\perp}{\sqrt{A}}, 0\right) = \frac{Nq_\perp^2}{2\pi^2 Av}\int_0^{\Lambda_{\rm UV}} dk_\perp k_\perp^3\left[\left(1 + 2\frac{k_\perp^4}{\Omega^2}\right)\right.$$
$$\left.\times \int_0^1 dx \frac{1}{x(1-x)\Omega^2 + k_\perp^4} - \frac{2}{\Omega^2}\right]. \tag{A27}$$

Carrying out the integration over x and using the transformation $k_\perp = \sqrt{|\Omega|}y$, we get

$$\Pi_d\left(i\Omega, \frac{q_\perp}{\sqrt{A}}, 0\right) = \frac{Nq_\perp^2}{\pi^2 Av}\int_0^{\frac{\Lambda_{\rm UV}}{\sqrt{|\Omega|}}} dy\, F_{d6}, \tag{A28}$$

where

$$F_{d6} = y^3\left[\frac{1 + 2y^4}{\sqrt{1 + 4y^4}}\ln\left(\frac{\sqrt{1 + 4y^4} + 1}{\sqrt{1 + 4y^4} - 1}\right) - 1\right]. \tag{A29}$$

As $y \to \infty$, the integrand becomes

$$F_{d6} \to \frac{1}{3y}, \tag{A30}$$

which allows us to express $\Pi_d(i\Omega, \frac{q_\perp}{\sqrt{A}}, 0)$ in the form

$$\Pi_d\left(i\Omega, \frac{q_\perp}{\sqrt{A}}, 0\right) \approx \frac{Nq_\perp^2}{\pi^2 Av}\left[a_3 + a_4 + \frac{1}{3}\ln\left(\frac{\Lambda_{\rm UV}}{\sqrt{|\Omega|}}\right)\right], \tag{A31}$$

where

$$a_3 = \int_0^1 dy\, F_{d6}, \tag{A32}$$

$$a_4 = \int_1^{+\infty} dy\left(F_{d6} - \frac{1}{3y}\right). \tag{A33}$$

Numerical calculations show that

$$a_3 \approx 0.192\,007, \quad a_4 \approx -0.011\,451\,9. \tag{A34}$$

Retaining the leading term, we approximately obtain

$$\Pi_d\left(i\Omega, \frac{q_\perp}{\sqrt{A}}, 0\right) \approx \frac{Nq_\perp^2}{3\pi^2 Av}\ln\left(\frac{\Lambda_{\rm UV}}{\sqrt{|\Omega|}}\right). \tag{A35}$$

d. Ansatz for $\Pi_d(i\Omega, \mathbf{q})$

Based on the polarization calculated in different limits, as shown in Eqs. (A18), (A26), and (A35), we find that the polarization can be approximated by the following ansatz:

$$\Pi_d\left(i\Omega, \frac{q_\perp}{\sqrt{A}}, \frac{q_z}{v}\right)$$
$$\approx N\left[\frac{q_\perp^2}{3\pi^2 Av}\ln\left(\frac{\Lambda_{\rm UV}}{(\Omega^2 + q_\perp^4)^{1/4}} + 1\right) + \frac{1}{64Av}\frac{q_z^2}{\sqrt{\Omega^2 + q_z^2}}\right]. \tag{A36}$$

Making the rescaling transformations

$$\frac{q_x}{\sqrt{A}} \to q_x, \quad \frac{q_y}{\sqrt{A}} \to q_y, \quad \frac{\Lambda_{\rm UV}}{\sqrt{A}} \to \Lambda_{\rm UV}, \quad \frac{q_z}{v} \to q_z, \tag{A37}$$

we further have

$$\Pi_d(i\Omega, q_\perp, q_z) \approx N\left[\frac{q_\perp^2}{3\pi^2 v}\ln\left(\frac{\sqrt{A}\Lambda_{\rm UV}}{(\Omega^2 + A^2 q_\perp^4)^{1/4}} + 1\right)\right.$$
$$\left.+ \frac{1}{64A}\frac{vq_z^2}{\sqrt{\Omega^2 + v^2 q_z^2}}\right]. \tag{A38}$$

This function will be used to compute the fermion self-energy.

In Fig. 10, we present a direct comparison between the approximate analytical expression (A38) and the exact one-loop polarization (A14). One can see that Eq. (A38) is very close to the exact one-loop polarization of double-Weyl fermions in the low-energy region.
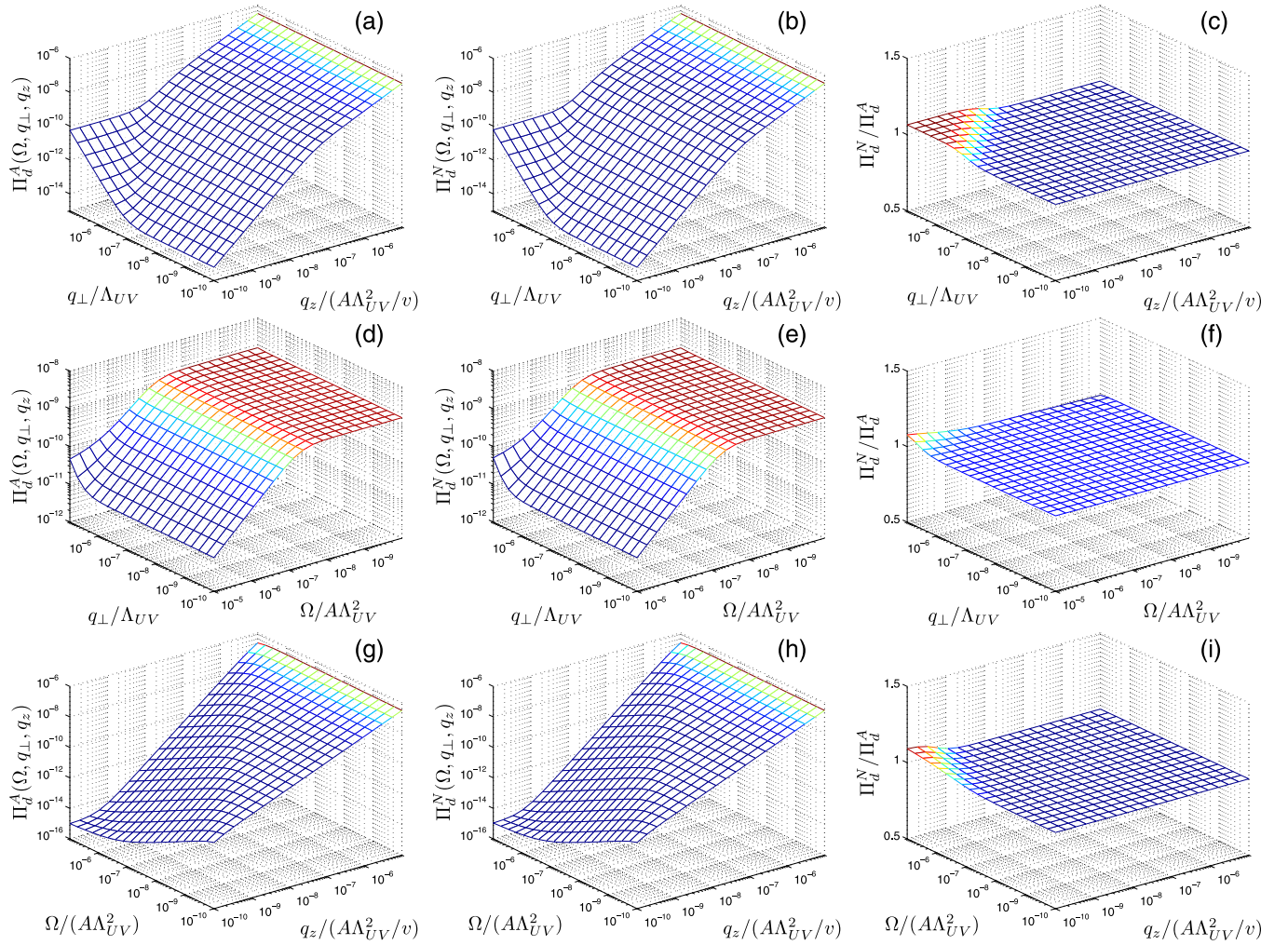
FIG. 10. Comparing the approximate expression of polarization with the exact polarization for double-Weyl fermions. Π_d^A represents the approximate expression of polarization given by Eq. (A38). Π_d^N is the numerical result of the polarization as shown in Eq. (A14). Dependence of Π_d^A, Π_d^N, and Π_d^N/Π_d^A on $q_\perp$ and q_z with $\Omega/A\Lambda_{\rm UV}^2 = 10^{-5}$ are shown in (a), (b), and (c). Dependence of Π_d^A, Π_d^N, and Π_d^N/Π_d^A on Ω and $q_\perp$ with $q_z/(A\Lambda_{\rm UV}^2/v) = 10^{-5}$ are displayed in (d), (e), and (f). Dependence of Π_d^A, Π_d^N, and Π_d^N/Π_d^A on Ω and q_z with $q_\perp/\Lambda_{\rm UV} = 10^{-5}$ are presented in (g), (h), and (i).

2. Polarization $\Pi_t(i\Omega, \mathbf{q})$ of triple-Weyl fermions

For triple-WSM, the polarization is given by

$$\Pi_t(i\Omega, \mathbf{q}) = -N \int \frac{d\omega}{2\pi} \int \frac{d^3\mathbf{k}}{(2\pi)^3} \text{Tr}[G_{t0}(i\omega, \mathbf{k})$$
$$\times G_{t0}(i\omega + i\Omega, \mathbf{k} + \mathbf{q})]. \quad \text{(A39)}$$

Substituting the fermion propagator Eq. (8) into Eq. (A39), we find that

$$\Pi_t\left(i\Omega, \frac{q_x}{B^{1/3}}, \frac{q_y}{B^{1/3}}, \frac{q_z}{v}\right) = \frac{2N}{B^{2/3}v} \int \frac{d\omega}{2\pi} \int \frac{d^3\mathbf{k}}{(2\pi)^3} \frac{F_{t1}^A}{F_{t1}^B}, \quad \text{(A40)}$$

where

$$F_{t1}^A = \omega(\omega + \Omega) - \sum_{i=1}^{3} g_i(\mathbf{k})g_i(\mathbf{k} + \mathbf{q}), \quad \text{(A41)}$$

$$F_{t1}^B = \left(\omega^2 + E_\mathbf{k}^2\right)\left[(\omega + \Omega)^2 + E_{\mathbf{k}+\mathbf{q}}^2\right]. \quad \text{(A42)}$$

Here, $g_1(\mathbf{k}) = (k_x^3 - 3k_x k_y^2)$, $g_2(\mathbf{k}) = (k_y^3 - 3k_y k_x^2)$, $g_3(\mathbf{k}) = k_z$, and $E_\mathbf{k} = \sqrt{k_\perp^6 + k_z^2}$. The above calculations are completed by using the following rescaling manipulations:

$$k_x \to \frac{k_x}{B^{1/3}}, \quad k_y \to \frac{k_y}{B^{1/3}}, \quad q_x \to \frac{q_x}{B^{1/3}},$$
$$q_y \to \frac{q_y}{B^{1/3}}, \quad k_z \to \frac{k_z}{v}, \quad q_z \to \frac{q_z}{v}. \quad \text{(A43)}$$

Introducing Feynman integral, we further rewrite the polarization as

$$\Pi_t\left(i\Omega, \frac{q_x}{B^{1/3}}, \frac{q_y}{B^{1/3}}, \frac{q_z}{v}\right)$$
$$= \frac{2N}{B^{2/3}v} \int_0^1 dx \int \frac{dk_x}{2\pi} \frac{dk_y}{2\pi} F_{t2}^A \int \frac{d^2\mathbf{K}}{(2\pi)^2} \frac{1}{\left(F_{t2}^B\right)^2}, \quad \text{(A44)}$$

where $\mathbf{K} = (\omega, k_z)$ and

$$F_{t2}^A = -x(1-x)\left(\Omega^2 - q_z^2\right) - g_1\left(\mathbf{k} - \frac{\mathbf{q}}{2}\right)g_1\left(\mathbf{k} + \frac{\mathbf{q}}{2}\right) - g_2\left(\mathbf{k} - \frac{\mathbf{k}}{2}\right)g_2\left(\mathbf{k} + \frac{\mathbf{q}}{2}\right),$$ (A45)

$$F_{t2}^B = K^2 + x(1-x)\left(\Omega^2 + q_z^2\right) + (1-x)\left(\mathbf{k} - \frac{\mathbf{q}}{2}\right)_\perp^6 + x\left(\mathbf{k} + \frac{\mathbf{q}}{2}\right)_\perp^6.$$ (A46)

Transformations $k_x \to k_x - \frac{q_x}{2}$ and $k_y \to k_y - \frac{q_y}{2}$ have been adopted in the above calculation. Making use of Eq. (A10), we integrate over $\mathbf{K}$ and obtain

$$\Pi_t\left(i\Omega, \frac{q_x}{B^{1/3}}, \frac{q_y}{B^{1/3}}, \frac{q_z}{v}\right) = \frac{N}{2\pi B^{2/3}v}\int_0^1 dx \int \frac{dk_x}{2\pi}\frac{dk_y}{2\pi}\left(\frac{F_{t3}^A}{F_{t3}^B} + 1\right),$$ (A47)

where

$$F_{t3}^A = -x(1-x)\left(\Omega^2 - q_z^2\right) - \left(k_\perp^2 - \frac{q_\perp^2}{4}\right)^3 + 3\left(k_\perp^2 - \frac{q_\perp^2}{4}\right)(k_x q_y - k_y q_x)^2,$$ (A48)

$$F_{t3}^B = x(1-x)\left(\Omega^2 + q_z^2\right) + \left(k_\perp^2 + \frac{q_\perp^2}{4}\right)^3 + 3\left(k_\perp^2 + \frac{q_\perp^2}{4}\right)(k_x q_x + k_y q_y)^2$$

$$- (1-2x)\left[3\left(k_\perp^2 + \frac{q_\perp^2}{4}\right)^2(k_x q_x + k_y q_y) + (k_x q_x + k_y q_y)^3\right].$$ (A49)

In order to regularize the polarization, we have used $\Pi_t(i\Omega, \frac{q_x}{B^{1/3}}, \frac{q_y}{B^{1/3}}, \frac{q_z}{v}) - \Pi_t(0,0,0,0)$ to replace $\Pi_t(i\Omega, \frac{q_x}{B^{1/3}}, \frac{q_y}{B^{1/3}}, \frac{q_z}{v})$. In the polar coordinates, the polarization can be further converted to

$$\Pi_t\left(i\Omega, \frac{q_\perp}{B^{1/3}}, \frac{q_z}{v}\right) = \frac{N}{8\pi^3 B^{2/3}v}\int_0^1 dx \int_0^{\Lambda_{UV}} dk_\perp k_\perp \int_0^{2\pi} d\theta\left(\frac{F_{4t}^A}{F_{4t}^B} + 1\right),$$ (A50)

where

$$F_{4t}^A = -x(1-x)\left(\Omega^2 - q_z^2\right) - \left(k_\perp^2 - \frac{q_\perp^2}{4}\right)^3 + 3\left(k_\perp^2 - \frac{q_\perp^2}{4}\right)k_\perp^2 q_\perp^2 \sin^2(\theta),$$ (A51)

$$F_{4t}^B = x(1-x)\left(\Omega^2 + q_z^2\right) + \left(k_\perp^2 + \frac{q_\perp^2}{4}\right)^3 + 3\left(k_\perp^2 + \frac{q_\perp^2}{4}\right)k_\perp^2 q_\perp^2 \cos^2(\theta)$$

$$- (1-2x)\left[3\left(k_\perp^2 + \frac{q_\perp^2}{4}\right)^2 k_\perp q_\perp \cos(\theta) + k_\perp^3 q_\perp^3 \cos^3(\theta)\right].$$ (A52)

Similar to the case of double-WSM, we need to analyze the asymptotic behavior of the above polarization in several limits.

a. $q_\perp = 0$

In the limit $q_\perp = 0$, the polarization takes the form

$$\Pi_t\left(i\Omega, 0, \frac{q_z}{v}\right) = \frac{N}{2\pi^2 B^{2/3}v}q_z^2\int_0^1 dx\, x(1-x)\int_0^{\Lambda_{UV}} dk_\perp k_\perp \frac{1}{x(1-x)\left(\Omega^2 + q_z^2\right) + k_\perp^6}.$$ (A53)

Extending the upper limit of the integration over $k_\perp$ to infinity, we find that

$$\Pi_t\left(i\Omega, 0, \frac{q_z}{v}\right) = c_t \frac{N}{B^{2/3}v}\frac{q_z^2}{\left(\Omega^2 + q_z^2\right)^{2/3}},$$ (A54)

where

$$c_t = \frac{2^{1/3}\pi^{1/2}}{90\Gamma(5/6)\Gamma(2/3)}.$$ (A55)

b. $\Omega = 0$ and $q_z = 0$

When $\Omega = 0$ and $q_z = 0$, after integrating over x and making the transformation $k_\perp = q_\perp y$, the polarization

becomes

$$\Pi_t\left(0, \frac{q_\perp}{B^{1/3}}, 0\right) = \frac{Nq_\perp^2}{4\pi^3 B^{2/3}v}\int_0^{\frac{\pi}{2}} d\theta \int_0^{\frac{\Lambda_{UV}}{q_\perp}} dy\, F_{t5},$$ (A56)

where

$$F_{t5} = 2y + 3\frac{-\left(y^2 - \frac{1}{4}\right)^3 + 3\left(y^2 - \frac{1}{4}\right)y^2 \sin^2(\theta)}{3\left(y^2 + \frac{1}{4}\right)^2 \cos(\theta) + y^2 \cos^3(\theta)}$$

$$\times \ln\left(\frac{y^2 + \frac{1}{4} + y\cos(\theta)}{y^2 + \frac{1}{4} - y\cos(\theta)}\right).$$ (A57)

As $y \to \infty$, the integrand can be simplified as

$$F_{t5} \to \frac{6 - 3\cos(2\theta)}{y}. \tag{A58}$$

In the low-energy region, this polarization is simplified to

$$\Pi_t\left(0, \frac{q_\perp}{B^{1/3}}, 0\right) \approx \frac{Nq_\perp^2}{4\pi^3 B^{2/3} v}\left[a_5 + a_6 + 3\pi \ln\left(\frac{\Lambda_{\mathrm{UV}}}{q_\perp}\right)\right], \tag{A59}$$

where

$$a_5 = \int_0^{\frac{\pi}{2}} d\theta \int_0^1 dy\, F_{t5}, \tag{A60}$$

$$a_6 = \int_0^{\frac{\pi}{2}} d\theta \int_1^{+\infty} dy\left[F_{t5} - \frac{6 - 3\cos(2\theta)}{y}\right]. \tag{A61}$$

$$\Pi_t\left(i\Omega, \frac{q_\perp}{B^{1/3}}, 0\right) = \frac{9Nq_\perp^2}{8\pi^2 B^{2/3} v} \int dk_\perp k_\perp^5\left[\left(1 + 2\frac{k_\perp^6}{\Omega^2}\right)\int_0^1 dx\, \frac{1}{x(1-x)\Omega^2 + k_\perp^6} - \frac{2}{\Omega^2}\right]. \tag{A64}$$

Performing the integration over x and employing the transformation $k_\perp = |\Omega|^{1/3} y$, we further obtain

$$\Pi_t\left(i\Omega, \frac{q_\perp}{B^{1/3}}, 0\right) = \frac{9Nq_\perp^2}{4\pi^2 B^{2/3} v} \int_0^{\frac{\Lambda_{\mathrm{UV}}}{|\Omega|^{1/3}}} dy\, F_{t6}, \tag{A65}$$

where

$$F_{t6} = y^5\left[\frac{1 + 2y^6}{\sqrt{1 + 4y^6}} \ln\left(\frac{\sqrt{1 + 4y^6} + 1}{\sqrt{1 + 4y^6} - 1}\right) - 1\right]. \tag{A66}$$

As $y \to \infty$, the integrand becomes

$$F_{t6} \to \frac{1}{3y}, \tag{A67}$$

thus, we simplify the polarization to

$$\Pi_t\left(i\Omega, \frac{q_\perp}{B^{1/3}}, 0\right) \approx \frac{9Nq_\perp^2}{4\pi^2 B^{2/3} v}\left[a_7 + a_8 + \frac{1}{3} \ln\left(\frac{\Lambda_{\mathrm{UV}}}{|\Omega|^{1/3}}\right)\right], \tag{A68}$$

where

$$a_7 = \int_0^1 dy\, F_{t6}, \tag{A69}$$

$$a_8 = \int_1^{+\infty} dy\left(F_{t6} - \frac{1}{3y}\right). \tag{A70}$$

The values of a_7 and a_8 are

$$a_7 \approx 0.128\,005, \quad a_8 \approx -0.007\,634\,6. \tag{A71}$$

Keeping the leading contribution, the polarization is finally given by

$$\Pi_t\left(\Omega, \frac{q_\perp}{B^{1/3}}, 0\right) \approx \frac{3Nq_\perp^2}{4\pi^2 B^{2/3} v} \ln\left(\frac{\Lambda_{\mathrm{UV}}}{|\Omega|^{1/3}}\right). \tag{A72}$$

Numerical calculations lead to

$$a_5 \approx 1.9333, \quad a_6 \approx -3.289\,25. \tag{A62}$$

Retaining the leading term, we get

$$\Pi_t\left(0, \frac{q_\perp}{B^{1/3}}, 0\right) = \frac{3Nq_\perp^2}{4\pi^2 B^{2/3} v} \ln\left(\frac{\Lambda_{\mathrm{UV}}}{q_\perp}\right). \tag{A63}$$

c. $q_z = 0$ and $q_\perp^3 \ll \Omega$

For $q_z = 0$ and $q_\perp^3 \ll \Omega$, the polarization can be approximated by

According to the numerical results shown in Fig. 11, we can see that the above approximate analytical expression (A73) is very close to the exact one-loop polarization of triple-Weyl fermions in the low-energy region.

d. Ansatz for $\Pi_t(i\Omega, \mathbf{q})$

Based on the polarization calculated in different limits, as shown in Eqs. (A54), (A63), and (A72), the polarization can be approximated by the ansatz

$$\Pi_t(i\Omega, q_\perp, q_z) = N\left[\frac{3q_\perp^2}{4\pi^2 v} \ln\left(\frac{B^{1/3}\Lambda_{\mathrm{UV}}}{(\Omega^2 + B^2 q_\perp^6)^{1/6}} + 1\right) + c_t \frac{1}{B^{2/3}} \frac{v q_z^2}{(\Omega^2 + v^2 q_z^2)^{2/3}}\right]. \tag{A73}$$

APPENDIX B: FERMION SELF-ENERGY

We now compute the fermion self-energy functions caused by the Coulomb interaction, first for double-Weyl fermions and then for triple-Weyl fermions.

1. Self-energy of double-Weyl fermions

To the leading order of $1/N$ expansion, the self-energy of double-Weyl fermions due to Coulomb interaction is defined as

$$\Sigma_d(i\omega, \mathbf{k}) = \int' \frac{d\Omega}{2\pi} \frac{d^3\mathbf{q}}{(2\pi)^3} G_{d0}(i\omega + i\Omega, \mathbf{k} + \mathbf{q}) V_d(i\Omega, \mathbf{q}), \tag{B1}$$
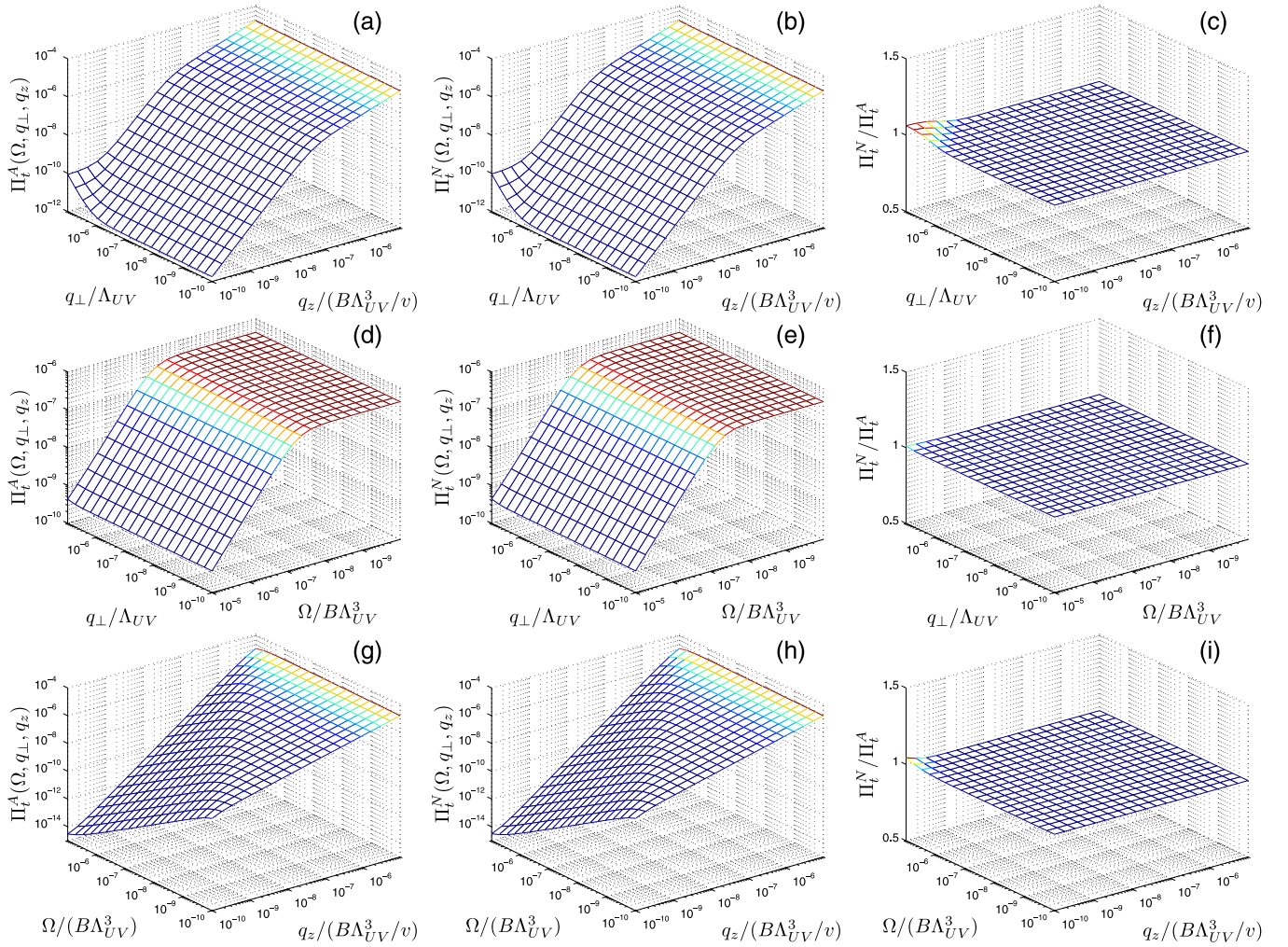
FIG. 11. Comparing the approximate expression of polarization with the exact polarization for triple-Weyl fermions. Π_t^A represents the approximate expression of polarization given by Eq. (A73). Π_t^N is the numerical result of the polarization as shown in Eq. (A50). Dependence of Π_t^A, Π_t^N, and Π_t^N/Π_t^A on $q_\perp$ and q_z with $\Omega/B\Lambda_{\mathrm{UV}}^3 = 10^{-5}$ are shown in (a), (b), and (c). Dependence of Π_t^A, Π_t^N, and Π_t^N/Π_t^A on Ω and $q_\perp$ with $q_z/(B\Lambda_{\mathrm{UV}}^3/v) = 10^{-5}$ are displayed in (d), (e), and (f). Dependence of Π_t^A, Π_t^N, and Π_t^N/Π_t^A on Ω and q_z with $q_\perp/\Lambda_{\mathrm{UV}} = 10^{-5}$ are presented in (g), (h), and (i).

where the dressed Coulomb interaction function is

$$V_d(i\Omega, \mathbf{q}) = \frac{1}{V_0^{-1}(\mathbf{q}) + \Pi_d(i\Omega, \mathbf{q})} = \frac{1}{\frac{q_\perp^2 + \xi q_z^2}{4\pi\alpha v} + \frac{Nq_\perp^2}{3\pi^2 v} \ln\left(\frac{\sqrt{A}\Lambda_{\mathrm{UV}}}{(\Omega^2 + A^2 q_\perp^4)^{1/4}} + 1\right) + \frac{N}{64A} \frac{vq_z^2}{\sqrt{\Omega^2 + v^2 q_z^2}}}. \tag{B2}$$

We then substitute Eq. (7) into Eq. (B1), and expand $\Sigma_d(i\omega, \mathbf{k})$ in powers of small values of $i\omega$, k_x, k_y, and k_z. To the leading order, the self-energy can be expressed as

$$\Sigma_d(i\omega, \mathbf{k}) \approx i\omega\Sigma_{d1} - A[d_1(\mathbf{k})\sigma_x + d_2(\mathbf{k})\sigma_y]\Sigma_{d2} - vk_z\sigma_z\Sigma_{d3}, \tag{B3}$$

where

$$\Sigma_{d1} = \frac{1}{8\pi^3} \int' d\Omega\, dq_\perp q_\perp dq_z \frac{\Omega^2 - A^2 q_\perp^4 - v^2 q_z^2}{\left(\Omega^2 + A^2 q_\perp^4 + v^2 q_z^2\right)^2} V_d(i\Omega, \mathbf{q}), \tag{B4}$$

$$\Sigma_{d2} = \frac{1}{8\pi^3} \int' d\Omega\, dq_\perp q_\perp dq_z \left[\frac{\Omega^2 - 4A^2 q_\perp^4 + v^2 q_z^2}{\left(\Omega^2 + A^2 q_\perp^4 + v^2 q_z^2\right)^2} + \frac{4A^4 q_\perp^8}{\left(\Omega^2 + A^2 q_\perp^4 + v^2 q_z^2\right)^3}\right] V_d(i\Omega, \mathbf{q}), \tag{B5}$$

$$\Sigma_{d3} = \frac{1}{8\pi^3} \int' d\Omega\, dq_\perp q_\perp dq_z \frac{\Omega^2 + A^2 q_\perp^4 - v^2 q_z^2}{\left(\Omega^2 + A^2 q_\perp^4 + v^2 q_z^2\right)^2} V_d(i\Omega, \mathbf{q}). \tag{B6}$$

Here, we adopt the following integration ranges:

$$-\infty < \Omega < \infty, \quad b\Lambda < E_d < \Lambda, \tag{B7}$$

with $E_d = \sqrt{A^2 q_\perp^4 + v^2 q_z^2}$ where $b = e^{-\ell}$. If we define

$$E = \sqrt{A^2 q_\perp^4 + v^2 q_z^2}, \quad \kappa = \frac{A q_\perp^2}{v|q_z|}, \tag{B8}$$

then we can write $q_\perp$ and q_z as

$$q_\perp = \frac{\sqrt{\kappa}\sqrt{E}}{\sqrt{A}(1+\kappa^2)^{1/4}}, \quad |q_z| = \frac{E}{v\sqrt{1+\kappa^2}}. \tag{B9}$$

Therefore, the integration over $q_\perp$ and q_z can be converted to the integration over E and κ, by invoking the relation

$$dq_\perp d|q_z| = \left\| \begin{matrix} \frac{\partial q_\perp}{\partial E} & \frac{\partial q_\perp}{\partial \kappa} \\ \frac{\partial |q_z|}{\partial E} & \frac{\partial |q_z|}{\partial \kappa} \end{matrix} \right\| dE\, d\kappa = \frac{\sqrt{E}}{2v\sqrt{A}\sqrt{\kappa}(1+\kappa^2)^{3/4}} dE\, d\kappa. \tag{B10}$$

Using the transformations given by Eqs. (B9) and (B10), we calculate Eqs. (B4)–(B6) along with the RG scheme (B7), and eventually obtain

$$\Sigma_{d1} = C_{d1}\ell, \quad \Sigma_{d2} = C_{d2}\ell, \quad \Sigma_{d3} = C_{d3}\ell, \tag{B11}$$

where

$$C_{d1} = \frac{1}{8\pi^3} \int_{-\infty}^{+\infty} dx \int_0^{+\infty} d\kappa \frac{1}{(1+\kappa^2)^{1/2}} \frac{x^2-1}{(x^2+1)^2} \mathcal{G}_d(x,\kappa), \tag{B12}$$

$$C_{d2} = \frac{1}{8\pi^3} \int_{-\infty}^{+\infty} dx \int_0^{+\infty} d\kappa \frac{1}{(1+\kappa^2)^{3/2}} \left[\frac{x^2(1+\kappa^2)-4\kappa^2+1}{(x^2+1)^2} + \frac{4\kappa^4}{(1+\kappa^2)(x^2+1)^3} \right] \mathcal{G}_d(x,\kappa), \tag{B13}$$

$$C_{d3} = \frac{1}{8\pi^3} \int_{-\infty}^{+\infty} dx \int_0^{+\infty} d\kappa \frac{1}{(1+\kappa^2)^{3/2}} \frac{x^2(1+\kappa^2)+\kappa^2-1}{(x^2+1)^2} \mathcal{G}_d(x,\kappa), \tag{B14}$$

with

$$\mathcal{G}_d^{-1}(x,\kappa) = \frac{1}{4\pi\alpha} \left(\kappa + \frac{\beta_d}{(1+\kappa^2)^{1/2}} \right) + N \left[\frac{\kappa}{3\pi^2} \ln \left(\frac{\gamma_d e^{\frac{\ell}{2}}(1+\kappa^2)^{1/4}}{[x^2(1+\kappa^2)+\kappa^2]^{1/4}} + 1 \right) + \frac{1}{64} \frac{1}{\sqrt{x^2(1+\kappa^2)+1}} \right]. \tag{B15}$$

Here, β_d and γ_d are defined by $\beta_d = \frac{\zeta A\Lambda}{v^2}$ and $\gamma_d = \frac{\sqrt{A}\Lambda_{\mathrm{UV}}}{\sqrt{\Lambda}}$, respectively.

2. Self-energy of triple-Weyl fermions

To the leading order of $1/N$ expansion, the self-energy of triple-Weyl fermions induced by the long-range Coulomb interaction is given by

$$\Sigma_t(i\omega, \mathbf{k}) = \int' \frac{d\Omega}{2\pi} \frac{d^3\mathbf{q}}{(2\pi)^3} G_{t0}(i\omega+i\Omega, \mathbf{k}+\mathbf{q}) V_t(i\Omega, \mathbf{q}), \tag{B16}$$

where

$$V_t(i\Omega, \mathbf{q}) = \frac{1}{V_0^{-1}(\mathbf{q}) + \Pi_t(i\Omega, \mathbf{q})} = \frac{1}{\frac{q_\perp^2+\zeta q_z^2}{4\pi\alpha v} + \frac{3Nq_\perp^2}{4\pi^2 v}\ln\left(\frac{B^{1/3}\Lambda_{\mathrm{UV}}}{(\Omega^2+B^2 q_\perp^6)^{1/6}}+1\right) + c_t \frac{N}{B^{2/3}} \frac{v q_z^2}{(\Omega^2+v^2 q_z^2)^{2/3}}}. \tag{B17}$$

After substituting Eq. (8) into Eq. (B16), and expanding $\Sigma_t(\omega, \mathbf{k})$ in powers of small $i\omega$, k_x, k_y, and k_z up to the leading order, we get

$$\Sigma_t(i\omega, \mathbf{k}) \approx i\omega \Sigma_{t1} - B[g_1(\mathbf{k})\sigma_x + g_2(\mathbf{k})\sigma_y]\Sigma_{t2} - vk_z\sigma_z\Sigma_{t3}, \tag{B18}$$

where

$$\Sigma_{t1} = \frac{1}{8\pi^3} \int' d\Omega \, dq_\perp q_\perp dq_z \frac{\Omega^2 - B^2 q_\perp^6 - v^2 q_z^2}{(\Omega^2 + B^2 q_\perp^6 + v^2 q_z^2)^2} V_t(i\Omega, \mathbf{q}), \tag{B19}$$

$$\Sigma_{t2} = \frac{1}{8\pi^3} \int' d\Omega \, dq_\perp q_\perp dq_z \left[\frac{\Omega^2 - 18B^2 q_\perp^6 + v^2 q_z^2}{(\Omega^2 + B^2 q_\perp^6 + v^2 q_z^2)^2} + \frac{45B^4 q_\perp^{12}}{(\Omega^2 + B^2 q_\perp^6 + v^2 q_z^2)^3} - \frac{27B^6 q_\perp^{18}}{(\Omega^2 + B^2 q_\perp^6 + v^2 q_z^2)^4} \right] V_t(i\Omega, \mathbf{q}), \tag{B20}$$

$$\Sigma_{t3} = \frac{1}{8\pi^3} \int' d\Omega \, dq_\perp q_\perp dq_z \frac{\Omega^2 + B^2 q_\perp^6 - v^2 q_z^2}{(\Omega^2 + B^2 q_\perp^6 + v^2 q_z^2)^2} V_t(i\Omega, \mathbf{q}). \tag{B21}$$

To make RG analysis, we consider the following ranges in energy:

$$-\infty < \Omega < \infty, \quad b\Lambda < E_t < \Lambda, \tag{B22}$$

with $E_t = \sqrt{B^2 q_\perp^6 + v^2 q_z^2}$. Making use of the definition

$$E = \sqrt{B^2 q_\perp^6 + v^2 q_z^2}, \quad \kappa = \frac{Bq_\perp^3}{v|q_z|}, \tag{B23}$$

we reexpress $q_\perp$ and q_z as

$$q_\perp = \frac{\kappa^{1/3} E^{1/3}}{B^{1/3}(1 + \kappa^2)^{1/6}}, \quad |q_z| = \frac{E}{v\sqrt{1 + \kappa^2}}. \tag{B24}$$

Now, the integration over $q_\perp$ and q_z can be transformed to the integration over E and κ through the relation

$$dq_\perp d|q_z| = \left\| \begin{matrix} \frac{\partial q_\perp}{\partial E} & \frac{\partial q_\perp}{\partial \kappa} \\ \frac{\partial |q_z|}{\partial E} & \frac{\partial |q_z|}{\partial \kappa} \end{matrix} \right\| dE \, d\kappa = \frac{E^{1/3}}{3v B^{1/3} \kappa^{2/3}(1 + \kappa^2)^{2/3}} dE \, d\kappa. \tag{B25}$$

By virtue of Eqs. (B24) and (B25), we calculate Eqs. (B19)–(B21) and obtain

$$\Sigma_{t1} = C_{t1}\ell, \quad \Sigma_{t2} = C_{t2}\ell, \quad \Sigma_{t3} = C_{t3}\ell, \tag{B26}$$

where

$$C_{t1} = \frac{1}{12\pi^3} \int_{-\infty}^{+\infty} dx \int_0^{+\infty} d\kappa \frac{1}{\kappa^{1/3}(1 + \kappa^2)^{1/2}} \frac{x^2 - 1}{(x^2 + 1)^2} \mathcal{G}_t(x, \kappa), \tag{B27}$$

$$C_{t2} = \frac{1}{12\pi^3} \int_{-\infty}^{+\infty} dx \int_0^{+\infty} d\kappa \frac{1}{\kappa^{1/3}(1 + \kappa^2)^{3/2}} \left[\frac{x^2(1 + \kappa^2) - 18\kappa^2 + 1}{(x^2 + 1)^2} + \frac{45\kappa^4}{(x^2 + 1)^3(1 + \kappa^2)} - \frac{27\kappa^6}{(x^2 + 1)^4(1 + \kappa^2)^2} \right] \mathcal{G}_t(x, \kappa), \tag{B28}$$

$$C_{t3} = \frac{1}{12\pi^3} \int_{-\infty}^{+\infty} dx \int_0^{+\infty} d\kappa \frac{1}{\kappa^{1/3}(1 + \kappa^2)^{3/2}} \frac{x^2(1 + \kappa^2) + \kappa^2 - 1}{(x^2 + 1)^2} \mathcal{G}_t(x, \kappa), \tag{B29}$$

with

$$\mathcal{G}_t^{-1}(x, \kappa) = \frac{1}{4\pi\alpha} \left(\kappa^{2/3} + \frac{\beta_t}{(1 + \kappa^2)^{2/3}} \right) + N \left[\frac{3\kappa^{2/3}}{4\pi^2} \ln \left(\frac{\gamma_t e^{\frac{\ell}{3}}(1 + \kappa^2)^{1/6}}{[x^2(1 + \kappa^2) + \kappa^2]^{1/6}} + 1 \right) + c_t \frac{1}{[x^2(1 + \kappa^2) + 1]^{2/3}} \right]. \tag{B30}$$

Here, β_t and γ_t are defined by $\beta_t = \frac{\zeta B^{2/3} \Lambda^{4/3}}{v^2}$ and $\gamma_t = \frac{B^{1/3} \Lambda_{\text{UV}}}{\Lambda^{1/3}}$, respectively.

APPENDIX C: DERIVING RG EQUATIONS

We derive the coupled RG equations for double- and triple-WSMs in order.

1. Double-WSM

We rewrite the free action of double-Weyl fermions as

$$S_{\psi_d}^0 = \int \frac{d\omega}{2\pi} \frac{d^3\mathbf{k}}{(2\pi)^3} \psi_d^\dagger(\omega, \mathbf{k})[i\omega - A[(d_1(\mathbf{k})\sigma_x + d_2(\mathbf{k})\sigma_y] - vk_z\sigma_z]\psi_d(\omega, \mathbf{k}). \tag{C1}$$

Including the fermion self-energy induced by the Coulomb interaction, this action becomes

$$S_{\psi_d} = \int \frac{d\omega}{2\pi} \frac{d^3\mathbf{k}}{(2\pi)^3} \psi_d^\dagger(\omega, \mathbf{k})[i\omega - A[d_1(\mathbf{k})\sigma_x + d_2(\mathbf{k})\sigma_y] - vk_z\sigma_z + \Sigma_d(i\omega, \mathbf{k})]\psi_d(\omega, \mathbf{k})$$

$$\approx \int \frac{d\omega}{2\pi} \frac{d^3\mathbf{k}}{(2\pi)^3} \psi_d^\dagger(\omega, \mathbf{k})[i\omega e^{C_{d1}\ell} - A[d_1(\mathbf{k})\sigma_x + d_2(\mathbf{k})\sigma_y]e^{C_{d2}\ell} - vk_z\sigma_z e^{C_{d3}\ell}]\psi_d(\omega, \mathbf{k}). \tag{C2}$$

We then make the following scaling transformations:

$$k_x = k_x' e^{-\frac{\ell}{2}}, \tag{C3}$$

$$k_y = k_y' e^{-\frac{\ell}{2}}, \tag{C4}$$

$$k_z = k_z' e^{-\ell}, \tag{C5}$$

$$\omega = \omega' e^{-\ell}, \tag{C6}$$

$$\psi_d = \psi_d' e^{(2-\frac{C_{d1}}{2})\ell}, \tag{C7}$$

$$A = A' e^{(C_{d1}-C_{d2})\ell}, \tag{C8}$$

$$v = v' e^{(C_{d1}-C_{d3})\ell}, \tag{C9}$$

which leads to

$$S_{\psi_d'} = \int \frac{d\omega'}{2\pi} \frac{d^3\mathbf{k}'}{(2\pi)^3} \psi_d'^\dagger(\omega', \mathbf{k}')[i\omega' - A'[d_1(\mathbf{k}')\sigma_x$$
$$+ d_2(\mathbf{k}')\sigma_y] - v'k_z'\sigma_z]\psi_d'(\omega', \mathbf{k}'). \tag{C10}$$

This action has the same form as the free action.

From Eq. (C7), the flow equation for the residue Z_f is

$$\frac{dZ_f}{d\ell} = -C_{d1}Z_f. \tag{C11}$$

According to Eqs. (C8) and (C9), we find that the flow equations of A and v are

$$\frac{dA}{d\ell} = (C_{d2} - C_{d1})A, \tag{C12}$$

$$\frac{dv}{d\ell} = (C_{d3} - C_{d1})v. \tag{C13}$$

The flow equations of other parameters α, β_d, and γ_d are

$$\frac{d\alpha}{d\ell} = (C_{d1} - C_{d3})\alpha, \tag{C14}$$

$$\frac{d\beta_d}{d\ell} = (C_{d1} + C_{d2} - 2C_{d3} - 1)\beta_d, \tag{C15}$$

$$\frac{d\gamma_d}{d\ell} = \frac{1}{2}(C_{d2} - C_{d1})\gamma_d. \tag{C16}$$

2. Triple-WSM

By repeating the same computational procedure employed in the case of double-WSM, we add the self-energy of triple-

Weyl fermions to the free action and then obtain

$$S_{\psi_t} = \int \frac{d\omega}{2\pi} \frac{d^3\mathbf{k}}{(2\pi)^3} \psi_t^\dagger(\omega, \mathbf{k})[i\omega e^{C_{t1}\ell} - B[g_1(\mathbf{k})\sigma_x$$
$$+ g_2(\mathbf{k})\sigma_y]e^{C_{t2}\ell} - vk_z\sigma_z e^{C_{t3}\ell}]\psi_t(\omega, \mathbf{k}). \tag{C17}$$

Making use of the scaling transformations

$$k_x = k_x' e^{-\frac{\ell}{3}}, \tag{C18}$$

$$k_y = k_y' e^{-\frac{\ell}{3}}, \tag{C19}$$

$$k_z = k_z' e^{-\ell}, \tag{C20}$$

$$\omega = \omega' e^{-\ell}, \tag{C21}$$

$$\psi_t = \psi_t' e^{(\frac{11}{6}-\frac{C_{t1}}{2})\ell}, \tag{C22}$$

$$B = B' e^{(C_{t1}-C_{t2})\ell}, \tag{C23}$$

$$v = v' e^{(C_{t1}-C_{t3})\ell}, \tag{C24}$$

the above action is converted to

$$S_{\psi_t'} = \int \frac{d\omega'}{2\pi} \frac{d^3\mathbf{k}'}{(2\pi)^3} \psi_t'^\dagger(\omega', \mathbf{k}')[i\omega' - B'[g_1(\mathbf{k}')\sigma_x$$
$$+ g_2(\mathbf{k}')\sigma_y] - v'k_z'\sigma_z]\psi_t'(\omega', \mathbf{k}'), \tag{C25}$$

which recovers the same form as the free action. From the transformations (C22)–(C24), we get the flow equations for Z_f, B, and v:

$$\frac{dZ_f}{d\ell} = -C_{t1}Z_f, \tag{C26}$$

$$\frac{dB}{d\ell} = (C_{t2} - C_{t1})B, \tag{C27}$$

$$\frac{dv}{d\ell} = (C_{t3} - C_{t1})v. \tag{C28}$$

The flow equations of α, β_t, and γ_t are given by

$$\frac{d\alpha}{d\ell} = (C_{t1} - C_{t3})\alpha, \tag{C29}$$

$$\frac{d\beta_t}{d\ell} = \left(\frac{4}{3}C_{t1} + \frac{2}{3}C_{t2} - 2C_{t3} - \frac{4}{3}\right)\beta_t, \tag{C30}$$

$$\frac{d\gamma_t}{d\ell} = \frac{1}{3}(C_{t2} - C_{t1})\gamma_t. \tag{C31}$$

APPENDIX D: IMPACT OF FINITE CHEMICAL POTENTIAL

As discussed in the main text, the unconventional non-FL state can by experimentally explored by measuring the fermion damping rate and spectral function in several candidate materials for double- and triple-WSMs. To observe the predicted non-FL behavior, the sample needs to be carefully prepared. In particular, the chemical potential μ should be made sufficiently small because the signature is sharpest at $\mu = 0$. At finite μ, the fermion DOS takes a finite value, and as such leads to static screening of long-range Coulomb interaction. We now make a brief remark on the impact of finite μ on the unconventional non-FL behavior.

For a double-WSM prepared at finite μ, the Matsubara fermion propagator becomes

$$G_{d0}(i\omega_n, \mathbf{k}) = \frac{1}{i\omega_n + \mu - \mathcal{H}_d(\mathbf{k})}, \qquad (D1)$$

where $\mathcal{H}_d(\mathbf{k}) = Ad_1(\mathbf{k})\sigma_x + Ad_2(\mathbf{k})\sigma_y + vk_z\sigma_z$. The retarded fermion propagator has the form

$$G_{d0}^{\text{ret}}(\omega, \mathbf{k}) = \frac{1}{\omega + \mu - \mathcal{H}_d(\mathbf{k}) + i\delta}, \qquad (D2)$$

which gives rise to the following spectral function:

$$\begin{aligned}
\mathcal{A}_d(\omega, \mathbf{k}) &= -\frac{1}{\pi}\text{Tr}\big[\text{Im}\big[G_{d0}^{\text{ret}}(\omega, \mathbf{k})\big]\big] \\
&= 2|\omega + \mu|\delta\big((\omega + \mu)^2 - E_d^2(\mathbf{k})\big), \quad (D3)
\end{aligned}$$

where $E_d(\mathbf{k}) = \sqrt{A^2 k_\perp^4 + v^2 k_z^2}$. The fermion DOS is given by

$$\rho_d(\omega) = N \int \frac{d^3\mathbf{k}}{(2\pi)^3}\mathcal{A}_d(\omega, \mathbf{k}) = \frac{N}{8\pi vA}|\omega + \mu|. \quad (D4)$$

Here, we have carried out the transformations shown in Eqs. (B8)–(B10). In the limit $\omega \to 0$, we have

$$\rho_d(0) = \frac{N|\mu|}{8\pi vA}. \qquad (D5)$$

In the limits of $\Omega = 0$ and $\mathbf{q} = 0$, the polarization function behaves as

$$\Pi_d(0, 0) = N \int \frac{d^3\mathbf{k}}{(2\pi)^3}\frac{1}{E_d(\mathbf{k})}\theta[|\mu| - E_d(\mathbf{k})]. \quad (D6)$$

Substituting $E_d(\mathbf{k})$ into this formula and employing the transformations (B8)–(B10), we obtain

$$\Pi_d(0, 0) = \frac{N|\mu|}{8\pi vA} = \rho_d(0). \qquad (D7)$$

In the case of triple-WSM, one can similarly get the retarded fermion propagator

$$G_{t0}^{\text{ret}}(\omega, \mathbf{k}) = \frac{1}{\omega + \mu - \mathcal{H}_t(\mathbf{k}) + i\delta}, \qquad (D8)$$

where $\mathcal{H}_t(\mathbf{k}) = Bg_1(\mathbf{k})\sigma_x + Bg_2(\mathbf{k})\sigma_y + vk_z\sigma_z$. The spectral function is

$$\begin{aligned}
\mathcal{A}_t(\omega, \mathbf{k}) &= -\frac{1}{\pi}\text{Tr}\big[\text{Im}\big[G_{t0}^{\text{ret}}(\omega, \mathbf{k})\big]\big] \\
&= 2|\omega + \mu|\delta\big((\omega + \mu)^2 - E_t^2(\mathbf{k})\big), \quad (D9)
\end{aligned}$$

where $E_t(\mathbf{k}) = \sqrt{B^2 k_\perp^6 + v^2 k_z^2}$. The fermion DOS is

$$\rho_t(\omega) = N \int \frac{d^3\mathbf{k}}{(2\pi)^3}\mathcal{A}_t(\omega, \mathbf{k}) = \frac{N\Gamma(1/3)|\omega + \mu|^{2/3}}{12\pi^{3/2}\Gamma(5/6)vB^{2/3}}, \qquad (D10)$$

which reduces to

$$\rho_t(0) = \frac{N\Gamma(1/3)|\mu|^{2/3}}{12\pi^{3/2}\Gamma(5/6)vB^{2/3}} \qquad (D11)$$

in the lowest-energy limit. Therefore, we have

$$\Pi_t(0, 0) = N \int \frac{d^3\mathbf{k}}{(2\pi)^3}\frac{1}{E_t(\mathbf{k})}\theta[|\mu| - E_t(\mathbf{k})] = \frac{3}{2}\rho_t(0). \qquad (D12)$$

From the above results, we know that the polarizations $\Pi_{d,t}$ always take certain finite value in the zero-energy (long-wavelength) limit. Consequently, the Coulomb interaction, described by the dressed function

$$V_{d,t}(i\Omega, \mathbf{q}) = \frac{1}{V_0^{-1}(\mathbf{q}) + \Pi_{d,t}(i\Omega, \mathbf{q})}, \qquad (D13)$$

is statically screened and becomes short ranged. Here, we provide a qualitative analysis for the behavior of fermion self-energy $\Sigma_{d,t}(i\omega, \mathbf{k})$ at $\mu \neq 0$.

At energies below the scale set by μ, the screened Coulomb interaction is relatively unimportant and only produces ordinary FL behavior. In contrast, at energies beyond the scale of μ, the static screening effect is unimportant, and the Coulomb interaction still induces unconventional non-FL behavior. Thus, increasing the energy scale drives a crossover from the FL regime to the non-FL regime. If one varies the temperature T, there is an analogous crossover between the FL and non-FL regimes: the system exhibits FL behavior at $kT < \mu$ and non-FL behavior $kT > \mu$. We notice that the crossover from a usual FL state to a singular FL state, in which Z_f approaches to a finite value in the lowest-energy limit but the fermion velocity receives singular renormalization, has been studied in DSMs at finite chemical potential [80,81]. In the double- and triple-WSMs considered in this paper, the unconventional non-FL state always has observable effects as long as the chemical potential is not large enough, as explained in Sec. V in more detail.

APPENDIX E: OBSERVABLE QUANTITIES FOR FREE FERMIONS

We now calculate the specific heat and dynamical conductivities for free double- and triple-Weyl fermions. The interaction-induced corrections will be included later.

1. Specific heat

a. Double-WSM

In the Matsubara formalism, the propagator of free double-Weyl fermions reads as

$$G_{d0}(i\omega_n, \mathbf{k}) = \frac{-i\omega_n + \mathcal{H}_d(\mathbf{k})}{\omega_n^2 + E_d^2(\mathbf{k})}, \qquad (E1)$$

where $\omega_n = (2n+1)\pi T$ with n being integers. The corresponding free energy is given by

$$F_f^d(T) = -2NT \sum_{\omega_n} \int \frac{d^3\mathbf{k}}{(2\pi)^3} \ln\left[\left[\omega_n^2 + E_d^2(\mathbf{k})\right]^{\frac{1}{2}}\right]. \quad (E2)$$

Carrying out frequency summation, one obtains

$$F_f^d(T) = -2N \int \frac{d^3\mathbf{k}}{(2\pi)^3} \left[E_d(\mathbf{k}) + 2T \ln\left(1 + e^{-\frac{E_d(\mathbf{k})}{T}}\right)\right], \quad (E3)$$

which is divergent due to the first term in the brackets. To regularize this divergence, we redefine $F_f^d(T) - F_f^d(0)$ as $F_f^d(T)$ and then get

$$F_f^d(T) = -4NT \int \frac{d^3\mathbf{k}}{(2\pi)^3} \ln\left(1 + e^{-\frac{E_d(\mathbf{k})}{T}}\right)$$
$$= -\frac{2NT}{\pi^2} \int dk_\perp d|k_z| k_\perp \ln\left(1 + e^{-\frac{E_d(\mathbf{k})}{T}}\right). \quad (E4)$$

Utilizing the integration transformations shown in Eqs. (B8)–(B10), the free energy becomes

$$F_f^d(T) = -\frac{NT}{\pi^2 vA} \int_0^{+\infty} dE\, E \ln\left(1 + e^{-\frac{E}{T}}\right)$$
$$\times \int_0^{+\infty} d\kappa \frac{1}{(1+\kappa^2)}$$
$$= -\frac{3\zeta(3)N}{8\pi vA} T^3. \quad (E5)$$

Then, it is easy to get the specific heat

$$C_v^d(T) = -T \frac{\partial^2 F_f^d(T)}{\partial T^2} = \frac{9\zeta(3)N}{4\pi vA} T^2. \quad (E6)$$

b. Triple-WSM

For triple-WSM, the free energy can be expressed as

$$F_f^t(T) = -\frac{2NT}{\pi^2} \int dk_\perp d|k_z| k_\perp \ln\left(1 + e^{-\frac{E_t(\mathbf{k})}{T}}\right). \quad (E7)$$

Carrying out the transformations of Eqs. (B23)–(B25), we rewrite $F_f^t(T)$ in the form

$$F_f^t(T) = -\frac{2NT}{3\pi^2 vB^{2/3}} \int_0^{+\infty} dE\, E^{2/3} \ln\left(1 + e^{-\frac{E}{T}}\right)$$
$$\times \int_0^{+\infty} d\kappa \frac{1}{\kappa^{1/3}(1+\kappa^2)^{5/6}}$$
$$= -\frac{a_t N}{\pi^{3/2} vB^{2/3}} T^{8/3}, \quad (E8)$$

where the constant a_t is

$$a_t = \frac{1}{18}(4 - 2^{1/3})\zeta(8/3) \frac{\Gamma(1/3)\Gamma(2/3)}{\Gamma(5/6)}. \quad (E9)$$

The specific heat is

$$C_v^t(T) = -T \frac{\partial^2 F_f^t(T)}{\partial T^2} = \frac{40 a_t N}{9\pi^{3/2} vB^{2/3}} T^{5/3}. \quad (E10)$$

2. Dynamical conductivities

The energy-dependence dynamical conductivities will be computed by using the Kubo formula.

a. Double-WSM

In the Matsubara formalism, the current-current correlation function for double-Weyl fermions can be written as

$$\Pi_{ij}^d(i\Omega_m) = -e^2 T \sum_{\omega_n} \int \frac{d^3\mathbf{k}}{(2\pi)^3} \text{Tr}\big[\gamma_i^d(\mathbf{k}) G_{d0}(i\omega_n, \mathbf{k})$$
$$\times \gamma_j^d(\mathbf{k}) G_{d0}(i\omega_n + i\Omega_m, \mathbf{k})\big]. \quad (E11)$$

Here, γ_i^d is given by

$$\gamma_i^d = \frac{\partial \mathcal{H}_d}{\partial k_i}, \quad (E12)$$

with $\mathcal{H}_d$ being the Hamiltonian density

$$\mathcal{H}_d = A(k_x^2 - k_y^2)\sigma_x + 2Ak_xk_y\sigma_y + vk_z\sigma_z. \quad (E13)$$

It is easy to verify that

$$\gamma_x^d = \frac{\partial \mathcal{H}_d}{\partial k_x} = 2Ak_x\sigma_x + 2Ak_y\sigma_y, \quad (E14)$$

$$\gamma_y^d = \frac{\partial \mathcal{H}_d}{\partial k_y} = -2Ak_y\sigma_x + 2Ak_x\sigma_y, \quad (E15)$$

$$\gamma_z^d = \frac{\partial \mathcal{H}_d}{\partial k_z} = v\sigma_z. \quad (E16)$$

Symmetry consideration reveals that the following identity

$$\Pi_{xx}^d = \Pi_{yy}^d \equiv \Pi_{\perp\perp}^d \quad (E17)$$

is satisfied. Therefore, we only need to calculate Π_{xx}^d and Π_{zz}^d, which are defined as follows:

$$\Pi_{xx}^d(i\Omega_m) = -e^2 T \sum_{\omega_n} \int \frac{d^3\mathbf{k}}{(2\pi)^3} \text{Tr}\big[\gamma_x^d G_{d0}(i\omega_n, \mathbf{k}) \gamma_x^d G_{d0}(i\omega_n + i\Omega_m, \mathbf{k})\big], \quad (E18)$$

$$\Pi_{zz}^d(i\Omega_m) = -e^2 T \sum_{\omega_n} \int \frac{d^3\mathbf{k}}{(2\pi)^3} \text{Tr}\big[\gamma_z^d G_{d0}(i\omega_n, \mathbf{k}) \gamma_z^d G_{d0}(i\omega_n + i\Omega_m, \mathbf{k})\big]. \quad (E19)$$

Employing the spectral representation

$$G_{d0}(i\omega_n, \mathbf{k}) = -\int_{-\infty}^{+\infty} \frac{d\omega_1}{\pi} \frac{\text{Im}\big[G_{d0}^{\text{ret}}(\omega_1, \mathbf{k})\big]}{i\omega_n - \omega_1}, \quad (E20)$$

we rewrite Π^d_{xx} and Π^d_{zz} as follows:

$$\Pi^d_{xx}(i\Omega_m) = -4A^2e^2 \int \frac{d^3\mathbf{k}}{(2\pi)^3} \int_{-\infty}^{+\infty} \frac{d\omega_1}{\pi} \int_{-\infty}^{+\infty} \frac{d\omega_2}{\pi} \{k_x^2 \text{Tr}[\sigma_x \text{Im}[G^{\text{ret}}_{d0}(\omega_1, \mathbf{k})]\sigma_x \text{Im}[G^{\text{ret}}_{d0}(\omega_2, \mathbf{k})]]$$

$$+ k_y^2 \text{Tr}[\sigma_y \text{Im}[G^{\text{ret}}_{d0}(\omega_1, \mathbf{k})]\sigma_y \text{Im}[G^{\text{ret}}_{d0}(\omega_2, \mathbf{k})]]\} \frac{n_F(\omega_1) - n_F(\omega_2)}{\omega_1 - \omega_2 + i\Omega_m}, \tag{E21}$$

$$\Pi^d_{zz}(i\Omega_m) = -v^2e^2 \int \frac{d^3\mathbf{k}}{(2\pi)^3} \int_{-\infty}^{+\infty} \frac{d\omega_1}{\pi} \int_{-\infty}^{+\infty} \frac{d\omega_2}{\pi} \text{Tr}[\sigma_z \text{Im}[G^{\text{ret}}_{d0}(\omega_1, \mathbf{k})]\sigma_z \text{Im}[G^{\text{ret}}_{d0}(\omega_2, \mathbf{k})]] \frac{n_F(\omega_1) - n_F(\omega_2)}{\omega_1 - \omega_2 + i\Omega_m}, \tag{E22}$$

where $n_F(x) = \frac{1}{e^{x/T}+1}$. The expression of $\text{Im}[G^{\text{ret}}_{d0}(\omega, \mathbf{k})]$ is given by

$$\text{Im}[G^{\text{ret}}_{d0}(\omega, \mathbf{k})] = -\pi \, \text{sgn}(\omega)(\omega + \mathcal{H}_d)\frac{1}{2E_d(\mathbf{k})}[\delta[\omega + E_d(\mathbf{k})] + \delta[\omega - E_d(\mathbf{k})]]. \tag{E23}$$

We then carry out analytical continuation $i\Omega_m \to \Omega + i\delta$, and get the imaginary parts:

$$\text{Im}[\Pi^{d,\text{ret}}_{xx}(\Omega, T)] = 4A^2e^2 \int \frac{d^3\mathbf{k}}{(2\pi)^3} \int_{-\infty}^{+\infty} \frac{d\omega_1}{\pi} \{k_x^2 \text{Tr}[\sigma_x \text{Im}[G^{\text{ret}}_{d0}(\omega_1, \mathbf{k})]\sigma_x \text{Im}[G^{\text{ret}}_{d0}(\omega_1 + \Omega, \mathbf{k})]]$$

$$+ k_y^2 \text{Tr}[\sigma_y \text{Im}[G^{\text{ret}}_{d0}(\omega_1, \mathbf{k})]\sigma_y \text{Im}[G^{\text{ret}}_{d0}(\omega_1 + \Omega, \mathbf{k})]]\} [n_F(\omega_1) - n_F(\omega_1 + \Omega)], \tag{E24}$$

$$\text{Im}[\Pi^{t,\text{ret}}_{zz}(\Omega, T)] = v^2e^2 \int \frac{d^3\mathbf{k}}{(2\pi)^3} \int_{-\infty}^{+\infty} \frac{d\omega_1}{\pi} \text{Tr}[\sigma_z \text{Im}[G^{\text{ret}}_{d0}(\omega_1, \mathbf{k})]\sigma_z \text{Im}[G^{\text{ret}}_{d0}(\omega_1 + \Omega, \mathbf{k})]] [n_F(\omega_1) - n_F(\omega_1 + \Omega)]. \tag{E25}$$

The formula $\frac{1}{x+i\delta} = \mathcal{P}\frac{1}{x} - i\pi\delta(x)$, where $\mathcal{P}$ stands for principal value, has been used in the above computation. According to Kubo formula, the dynamical conductivities are defined as

$$\sigma^d_{xx}(\Omega, T) = \frac{\text{Im}[\Pi^{d,\text{ret}}_{xx}(\Omega, T)]}{\Omega}, \tag{E26}$$

$$\sigma^d_{zz}(\Omega, T) = \frac{\text{Im}[\Pi^{d,\text{ret}}_{zz}(\Omega, T)]}{\Omega}. \tag{E27}$$

After carrying out analytical calculations, we arrive at the following compact expressions of conductivities:

$$\sigma^d_{xx}(\Omega, T) = c^d_1 \frac{e^2}{v}\delta(\Omega)T^2 + c^d_2 \frac{e^2}{v}|\Omega| \tanh\left(\frac{|\Omega|}{4T}\right), \tag{E28}$$

$$\sigma^d_{zz}(\Omega, T) = c^d_3 \frac{ve^2}{A}\delta(\Omega)T + c^d_4 \frac{ve^2}{A} \tanh\left(\frac{|\Omega|}{4T}\right), \tag{E29}$$

where

$$c^d_1 = \frac{1}{6\pi} \int_0^{+\infty} dx \, x^2 \frac{1}{\sinh^2\left(\frac{x}{2}\right)}, \tag{E30}$$

$$c^d_2 = \frac{1}{12\pi}, \tag{E31}$$

$$c^d_3 = \frac{1}{32} \int_0^{+\infty} dx \, x \frac{1}{\sinh^2\left(\frac{x}{2}\right)}, \tag{E32}$$

$$c^d_4 = \frac{1}{64}. \tag{E33}$$

The first term in the right-hand side of Eqs. (E28) and (E29) represents the Drude peak.

b. Triple-WSM

In the Matsubara formalism, the current-current correlation function for triple-Weyl fermions is

$$\Pi^t_{ij}(i\Omega_m) = -e^2 T \sum_{\omega_n} \int \frac{d^3\mathbf{k}}{(2\pi)^3} \text{Tr}[\gamma^t_i G_{t0}(i\omega_n, \mathbf{k})\gamma^t_j G_{t0}(i(\omega_n + \Omega_m), \mathbf{k})], \tag{E34}$$

where $\gamma_i^t = \frac{\partial \mathcal{H}_t}{\partial k_i}$ with the Hamiltonian density being $\mathcal{H}_t = B(k_x^3 - 3k_x k_y^2)\sigma_x + B(k_y^3 - 3k_y k_x^2)\sigma_y + v k_z \sigma_z$. It is easy to get

$$\gamma_x^t = \frac{\partial \mathcal{H}_t}{\partial k_x} = 3B(k_x^2 - k_y^2)\sigma_x - 6B k_x k_y \sigma_y, \tag{E35}$$

$$\gamma_y^t = \frac{\partial \mathcal{H}_t}{\partial k_y} = -6B k_x k_y \sigma_x + 3B(k_y^2 - k_x^2)\sigma_y, \tag{E36}$$

$$\gamma_z^t = \frac{\partial \mathcal{H}_t}{\partial k_z} = v \sigma_z. \tag{E37}$$

Due to the relation $\Pi_{xx}^t = \Pi_{yy}^t \equiv \Pi_{\perp\perp}^t$, we only calculate Π_{xx}^t and Π_{zz}^t, which take the form

$$\Pi_{xx}^t(i\Omega_m) = -e^2 T \sum_{\omega_n} \int \frac{d^3 \mathbf{k}}{(2\pi)^3} \text{Tr}\big[\gamma_x^t G_{t0}(i\omega_n, \mathbf{k})\gamma_x^t G_{t0}(i\omega_n + i\Omega_m, \mathbf{k})\big], \tag{E38}$$

$$\Pi_{zz}^t(i\Omega_m) = -e^2 T \sum_{\omega_n} \int \frac{d^3 \mathbf{k}}{(2\pi)^3} \text{Tr}\big[\gamma_z^t G_{t0}(i\omega_n, \mathbf{k})\gamma_z^t G_{t0}(i\omega_n + i\Omega_m, \mathbf{k})\big]. \tag{E39}$$

After performing a series of calculations, we find that the imaginary parts of retarded correlation functions Π_{xx}^t and Π_{zz}^t have the forms

$$\text{Im}\big[\Pi_{xx}^{t,\text{ret}}(\Omega, T)\big] = 9B^2 e^2 \int \frac{d^3 \mathbf{k}}{(2\pi)^3} \int_{-\infty}^{+\infty} \frac{d\omega_1}{\pi} \big\{(k_x^2 - k_y^2)^2 \text{Tr}\big[\sigma_x \text{Im}\big[G_{t0}^{\text{ret}}(\omega_1, \mathbf{k})\big]\sigma_x \text{Im}\big[G_{t0}^{\text{ret}}(\omega_1 + \Omega, \mathbf{k})\big]\big]$$
$$+ 4k_x^2 k_y^2 \text{Tr}\big[\sigma_y \text{Im}\big[G_{t0}^{\text{ret}}(\omega_1, \mathbf{k})\big]\sigma_y \text{Im}\big[G_{t0}^{\text{ret}}(\omega_1 + \Omega, \mathbf{k})\big]\big]\big\}[n_F(\omega_1) - n_F(\omega_1 + \Omega)], \tag{E40}$$

$$\text{Im}\big[\Pi_{zz}^{t,\text{ret}}(\Omega, T)\big] = v^2 e^2 \int \frac{d^3 \mathbf{k}}{(2\pi)^3} \int_{-\infty}^{+\infty} \frac{d\omega_1}{\pi} \text{Tr}\big[\sigma_z \text{Im}\big[G_{t0}^{\text{ret}}(\omega_1, \mathbf{k})\big]\sigma_z \text{Im}\big[G_{t0}^{\text{ret}}(\omega_1 + \Omega, \mathbf{k})\big]\big][n_F(\omega_1) - n_F(\omega_1 + \Omega)]. \tag{E41}$$

The expression of $\text{Im}[G_{t0}^{\text{ret}}(\omega, \mathbf{k})]$ reads as

$$\text{Im}\big[G_{t0}^{\text{ret}}(\omega, \mathbf{k})\big] = -\pi \, \text{sgn}(\omega)(\omega + \mathcal{H}_t)\frac{1}{2E_t(\mathbf{k})}[\delta[\omega + E_t(\mathbf{k})] + \delta[\omega - E_t(\mathbf{k})]]. \tag{E42}$$

The conductivities are given by

$$\sigma_{xx}^t(\Omega, T) = \frac{\text{Im}\big[\Pi_{xx}^{t,\text{ret}}(\Omega, T)\big]}{\Omega}, \tag{E43}$$

$$\sigma_{zz}^t(\Omega, T) = \frac{\text{Im}\big[\Pi_{zz}^{t,\text{ret}}(\Omega, T)\big]}{\Omega}. \tag{E44}$$

Substituting Eq. (E42) into Eqs. (E40), (E41), (E43), and (E44) leads to the following expressions:

$$\sigma_{xx}^t(\Omega, T) = c_1^t \frac{e^2}{v}\delta(\Omega)T^2 + c_2^t \frac{e^2}{v}|\Omega| \tanh\left(\frac{|\Omega|}{4T}\right), \tag{E45}$$

$$\sigma_{zz}^t(\Omega, T) = c_3^t \frac{v e^2}{B^{2/3}}\delta(\Omega)T^{\frac{2}{3}} + c_4^t \frac{v e^2}{B^{2/3}}\frac{1}{|\Omega|^{1/3}} \tanh\left(\frac{|\Omega|}{4T}\right), \tag{E46}$$

where

$$c_1^t = \frac{1}{4\pi} \int_0^{+\infty} dx \, x^2 \frac{1}{\sinh^2\left(\frac{x}{2}\right)}, \tag{E47}$$

$$c_2^t = \frac{1}{8\pi}, \tag{E48}$$

$$c_3^t = \frac{\Gamma(1/3)}{40\Gamma(5/6)\sqrt{\pi}} \int_0^{+\infty} dx \, x^{2/3} \frac{1}{\sinh^2\left(\frac{x}{2}\right)}, \tag{E49}$$

$$c_4^t = \frac{2^{1/3}\Gamma(1/3)}{120\Gamma(5/6)\sqrt{\pi}}. \tag{E50}$$

APPENDIX F: INTERACTION CORRECTIONS TO OBSERVABLE QUANTITIES

Now, we compute the interaction corrections to observable quantities by using the RG solutions of model parameters.

1. DOS

a. Double-WSM

For free double-Weyl fermions, the DOS is

$$\rho_d(\omega) \sim \frac{\omega}{vA}. \tag{F1}$$

Upon including interaction corrections, the constants A and v become ω dependent. We derive the following RG equation for $\rho_d(\omega)$:

$$\frac{d \ln(\rho_d(\omega))}{d \ln(\omega)} \sim 1 + C_{d1} + \frac{d \ln\left(\frac{1}{vA}\right)}{d \ln(\omega)}. \tag{F2}$$

On the right-hand side, the second term comes from the anomalous dimension of fermion field, and the third term is induced by the fermion dispersion renormalization. Recall that A and v satisfy the flow equations:

$$\frac{dA}{d\ell} = (C_{d2} - C_{d1})A, \tag{F3}$$

$$\frac{dv}{d\ell} = (C_{d3} - C_{d1})v. \tag{F4}$$

Using the transformation $\omega = \omega_0 e^{-\ell}$, where ω_0 is certain high-energy scale, the above equations are converted to

$$\frac{d\ln(A)}{d\ln(\omega)} = -(C_{d2} - C_{d1}), \tag{F5}$$

$$\frac{d\ln(v)}{d\ln(\omega)} = -(C_{d3} - C_{d1}). \tag{F6}$$

We then substitute Eqs. (F5) and (F6) into Eq. (F2), and obtain the RG equation for $\rho_d(\omega)$:

$$\frac{d\ln(\rho_d(\omega))}{d\ln(\omega)} \sim 1 - C_{d1} + C_{d2} + C_{d3}. \tag{F7}$$

b. Triple-WSM

For free triple-Weyl fermions, the DOS satisfies

$$\rho_t(\omega) \sim \frac{\omega^{2/3}}{vB^{2/3}}. \tag{F8}$$

The Coulomb interaction results in the following equation:

$$\frac{d\ln(\rho_t(\omega))}{d\ln(\omega)} \sim \frac{2}{3} + C_{t1} + \frac{d\ln\left(\frac{1}{vB^{2/3}}\right)}{d\ln(\omega)}. \tag{F9}$$

We employ the transformation $\omega = \omega_0 e^{-\ell}$ again, and get the RG equations for B and A:

$$\frac{d\ln(B)}{d\ln(\omega)} = -(C_{t2} - C_{t1}), \tag{F10}$$

$$\frac{d\ln(v)}{d\ln(\omega)} = -(C_{t3} - C_{t1}). \tag{F11}$$

Substituting Eqs. (F10) and (F11) into Eq. (F9) yields

$$\frac{d\ln(\rho_t(\omega))}{d\ln(\omega)} \sim 1 - \frac{2}{3}C_{t1} + \frac{2}{3}C_{t2} + C_{t3}. \tag{F12}$$

2. Specific heat

a. Double-WSM

The specific heat of free double-Weyl fermions exhibits the following T dependence:

$$C_v^d(T) \sim \frac{T^2}{vA}. \tag{F13}$$

The Coulomb interaction renormalized A and v, and as such leads to

$$\frac{d\ln(C_v^d(T))}{d\ln(T)} \sim 2 + \frac{d\ln\left(\frac{1}{vA}\right)}{d\ln(T)}. \tag{F14}$$

It is worth mentioning that the anomalous dimension of fermion field does not qualitatively modify the specific heat.

The qualitative interaction correction to specific heat originates merely from the fermion dispersion renormalization. To get the T dependence of A and v, we need to use the transformation $T = T_0 e^{-\ell}$, where T_0 is certain high-temperature scale. It is easy to convert Eqs. (F3) and (F4) into

$$\frac{d\ln(A)}{d\ln(T)} = -(C_{d2} - C_{d1}), \tag{F15}$$

$$\frac{d\ln(v)}{d\ln(T)} = -(C_{d3} - C_{d1}). \tag{F16}$$

Substituting Eqs. (F15) and (F16) into Eq. (F14), we obtain

$$\frac{d\ln(C_v^d(T))}{d\ln(T)} \sim 2 - 2C_{d1} + C_{d2} + C_{d3}. \tag{F17}$$

b. Triple-WSM

The specific heat for free triple-Weyl fermions is

$$C_v^t(T) \sim \frac{T^{5/3}}{vB^{2/3}}. \tag{F18}$$

One can show that the renormalized B and v satisfy the following equations:

$$\frac{d\ln(B)}{d\ln(T)} = -(C_{t2} - C_{t1}), \tag{F19}$$

$$\frac{d\ln(v)}{d\ln(T)} = -(C_{t3} - C_{t1}). \tag{F20}$$

The renormalized specific heat is found to have the form

$$\frac{d\ln(C_v^t(T))}{d\ln(T)} \sim \frac{5}{3} + \frac{d\ln\left(\frac{1}{vB^{2/3}}\right)}{d\ln(T)}$$
$$\sim \frac{5}{3} - \frac{5}{3}C_{t1} + \frac{2}{3}C_{t2} + C_{t3}. \tag{F21}$$

3. Dynamical conductivities

The dynamical conductivities can be calculated by following the steps adopted to compute DOS.

a. Double-WSM

The dynamical conductivity for free double-Weyl fermions within the x-y plane is

$$\sigma_{\perp\perp}^d(\Omega) \sim \frac{e^2}{v}|\Omega|. \tag{F22}$$

After incorporating the corrections due to the Coulomb interaction, we find that $\sigma_{\perp\perp}^d(\Omega)$ satisfies the following RG equation:

$$\frac{d\ln(\sigma_{\perp\perp}^d(\Omega))}{d\ln(\Omega)} \sim 1 + 2C_{d1} + \frac{d\ln\left(\frac{e^2}{v}\right)}{\ln(\Omega)}$$
$$\sim 1 + C_{d1} + C_{d3}. \tag{F23}$$

The dynamical conductivity along the z axis is

$$\sigma_{zz}^d(\Omega) \sim \frac{ve^2}{A}, \tag{F24}$$

which is altered by the Coulomb interaction to become

$$\frac{d \ln(\sigma_{zz}^d(\Omega))}{d \ln(\Omega)} \sim 2C_{d1} + \frac{d \ln\left(\frac{ve^2}{A}\right)}{\ln(\Omega)}$$

$$\sim 2C_{d1} + C_{d2} - C_{d3}. \qquad \text{(F25)}$$

b. Triple-WSM

The dynamical conductivities for free triple-Weyl fermions within the x-y plane and along the z axis are given by

$$\sigma_{\perp\perp}^t(\Omega) \sim \frac{e^2}{v}|\Omega|, \qquad \text{(F26)}$$

$$\sigma_{zz}^t(\Omega) \sim \frac{ve^2}{B^{2/3}} \frac{1}{|\Omega|^{1/3}}. \qquad \text{(F27)}$$

After including the interaction corrections, we find that

$$\frac{d \ln(\sigma_{\perp\perp}^t(\Omega))}{d \ln(\Omega)} \sim 1 + 2C_{t1} + \frac{d \ln\left(\frac{e^2}{v}\right)}{d \ln(\Omega)}$$

$$\sim 1 + C_{t1} + C_{t3}, \qquad \text{(F28)}$$

and that

$$\frac{d \ln(\sigma_{zz}^t(\Omega))}{d \ln(\Omega)} \sim -\frac{1}{3} + 2C_{t1} + \frac{d \ln\left(\frac{ve^2}{B^{2/3}}\right)}{d \ln(\Omega)}$$

$$\sim -\frac{1}{3} + \frac{7}{3}C_{t1} + \frac{2}{3}C_{t2} - C_{t3}. \qquad \text{(F29)}$$

[1] G. F. Giuliani and G. Vignale, *Quantum Theory of the Electron Liquid* (Cambridge University Press, Cambridge, 2005).

[2] P. Coleman, *Introduction to Many-Body Physics* (Cambridge University Press, Cambridge, 2015).

[3] A. J. Schofield, Non-Fermi liquids, Contemp. Phys. **40**, 95 (1999).

[4] C. M. Varma, Z. Nussinov, and W. v. Saarloos, Singular or non-Fermi liquids, Phys. Rep. **361**, 267 (2002).

[5] B. I. Halperin, P. A. Lee, and N. Read, Theory of the half-filled Landau level, Phys. Rev. B **47**, 7312 (1993).

[6] P. A. Lee, N. Nagaosa, and X.-G. Wen, Doping a Mott insulator: Physics of high-temperature superconductivity, Rev. Mod. Phys. **78**, 17 (2006).

[7] A. Abanov, A. V. Chubukov, and J. Schmalian, Quantum-critical theory of the spin-fermion model and its application to cuprates: Normal state analysis, Adv. Phys. **52**, 119 (2003).

[8] H. v. Löhneysen, A. Rosch, M. Vojta, and P. Wölfle, Fermi-liquid instabilites at magnetic quantum phase transitions, Rev. Mod. Phys. **79**, 1015 (2007).

[9] E. Fradkin, S. A. Kivelson, M. J. Lawler, J. P. Eisenstein, and A. P. Mackenzie, Nematic Fermi fluids in condensed matter physics, Annu. Rev. Condens. Matter Phys. **1**, 153 (2010).

[10] E. Fradkin, S. A. Kivelson, and J. M. Tranquada, Colloquium: Theory of intertwined orders in high temperature superconductors, Rev. Mod. Phys. **87**, 457 (2015).

[11] T. Shibauchi, A. Carrington, and Y. Matsuda, A quantum critical point lying beneath the superconducting dome in iron pnictides, Annu. Rev. Condens. Matter Phys. **5**, 113 (2014).

[12] C. M. Varma, P. B. Littlewood, S. Schmitt-Rink, E. Abrahams, and A. E. Ruckenstein, Phenomenology of the Normal State of Cu-O High-Temperature Superconductors, Phys. Rev. Lett. **63**, 1996 (1989).

[13] B. Keimer, S. A. Kivelson, M. R. Norman, S. Uchida, and J. Zaanen, From quantum matter to high-temperature superconductivity in copper oxides, Nature (London) **518**, 179 (2015).

[14] I. B. Sperstad, E. B. Stiansen, and A. Sudbø, Quantum criticality in a dissipative (2+1)-dimensional *XY* model of circulating currents in high-T_c cuprates, Phys. Rev. B **84**, 180503(R) (2011).

[15] M. Sutherland, R. P. Smith, N. Marcano, Y. Zou, S. E. Rowley, F. M. Grosche, N. Kimura, S. M. Hayden, S. Takashima, M. Nohara, and H. Takagi, Transport and thermodynamic evidence for a marginal Fermi-liquid state in ZrZn$_2$, Phys. Rev. B **85**, 035118 (2012).

[16] N. P. Armitage, E. J. Mele, and A. Vishwanath, Weyl and Dirac semimetals in three-dimensional solids, Rev. Mod. Phys. **90**, 015001 (2018).

[17] B.-J. Yang and N. Nagaosa, Classification of stable three-dimensional Dirac semimetals with nontrivial topology, Nat. Commun. **5**, 4898 (2014).

[18] G. Xu, H. Weng, Z. Wang, X. Dai, and Z. Fang, Chern Semimetal and the Quantized Anomalous Hall Effect in HgCr$_2$Se$_4$, Phys. Rev. Lett. **107**, 186806 (2011).

[19] C. Fang, M. J. Gilbert, X. Dai, and B. A. Bernevig, Multi-Weyl Topological Semimetals Stabilized by Point Group Symmetry, Phys. Rev. Lett. **108**, 266802 (2012).

[20] H.-H. Lai, Correlation effects in double-Weyl semimetals, Phys. Rev. B **91**, 235131 (2015).

[21] S.-K. Jian and H. Yao, Correlated double-Weyl semimetals with Coulomb interactions: Possible applications to HgCr$_2$Se$_4$ and SrSi$_2$, Phys. Rev. B **92**, 045121 (2015).

[22] B. Roy and J. D. Sau, Magnetic catalysis and axionic charge density wave in Weyl semimetals, Phys. Rev. B **92**, 125141 (2015).

[23] Q. Chen and G. A. Fiete, Thermoelectric transport in double-Weyl semimetals, Phys. Rev. B **93**, 155125 (2016).

[24] X. Dai, H.-Z. Lu, S.-Q. Shen, and H. Yao, Detecting monopole charge in Weyl semimetals via quantum interference transport, Phys. Rev. B **93**, 161110(R) (2016).

[25] S. Bera, J. D. Sau, and B. Roy, Dirty Weyl semimetals: Stability, phase transition, and quantum criticality, Phys. Rev. B **93**, 201302(R) (2016).

[26] L.-J. Zhai, P.-H. Chou, and C.-Y. Mou, Magnetic phases and unusual topological electronic structures of Weyl semimetals in strong interaction limit, Phys. Rev. B **94**, 125135 (2016).

[27] L. Lepori, I. C. Fulga, A. Trombettoni, and M. Burrello, Double Weyl points and Fermi arcs of topological semimetals in non-Abelian gauge potentials, Phys. Rev. A **94**, 053633 (2016).

[28] X. Li, B. Roy, and S. Das Sarma, Weyl fermions with arbitrary monopoles in magnetic fields: Landau levels, longitudinal magnetotransport, and density-wave ordering, Phys. Rev. B **94**, 195144 (2016).

[29] B. Sbierski, M. Trescher, E. J. Bergholtz, and P. W. Brouwer, Disordered double Weyl node: Comparison of transport and density of states calculations, Phys. Rev. B **95**, 115104 (2017).

[30] X.-Y. Mai, D.-W. Zhang, Z. Li, and S.-L. Zhu, Exploring topological double-Weyl semimetals with cold atoms in optical lattices, Phys. Rev. A **95**, 063616 (2017).

[31] S. Ahn, E. J. Mele, and H. Min, Optical conductivity of multi-Weyl semimetals, Phys. Rev. B **95**, 161112(R) (2017).

[32] S. Park, S. Woo, E. J. Mele, and H. Min, Semiclassical Boltzmann transport theory for multi-Weyl semimetals, Phys. Rev. B **95**, 161113(R) (2017).

[33] B. Roy, P. Goswami, and V. Juričić, Interacting Weyl fermions: Phases, phase transitions, and global phase diagram, Phys. Rev. B **95**, 201102(R) (2017).

[34] Z. Yan and Z. Wang, Floquet multi-Weyl points in crossing-nodal-line semimetals, Phys. Rev. B **96**, 041206(R) (2017).

[35] Z.-M. Huang, J. Zhou, and S.-Q. Shen, Topological responses from chiral anomaly in multi-Weyl semimetals, Phys. Rev. B **96**, 085201 (2017).

[36] T. Hayata, Y. Kikuchi, and Y. Tanizaki, Topological properties of the chiral magnetic effect in multi-Weyl semimetals, Phys. Rev. B **96**, 085112 (2017).

[37] Y. Sun and A.-M. Wang, Magneto-optical conductivity of double Weyl semimetals, Phys. Rev. B **96**, 085147 (2017).

[38] S.-K. Jian and H. Yao, Fermion-induced quantum critical points in three-dimensional Weyl semimetals, Phys. Rev. B **96**, 155112 (2017).

[39] E. V. Gorbar, V. A. Miransky, I. A. Shovkovy, and P. O. Sukhachov, Anomalous thermoelectric phenomena in lattice models of multi-Weyl semimetals, Phys. Rev. B **96**, 155138 (2017).

[40] J.-R. Wang, G.-Z. Liu, and C.-J. Zhang, Quantum phase transition and unusual critical behavior in multi-Weyl semimetals, Phys. Rev. B **96**, 165142 (2017).

[41] M. Ezawa, Merging of momentum-space monopoles by controlling Zeeman field: From cubic-Dirac to triple-Weyl fermion systems, Phys. Rev. B **96**, 161202(R) (2017).

[42] S.-X. Zhang, S.-K. Jian, and H. Yao, Correlated triple-Weyl semimetals with Coulomb interactions, Phys. Rev. B **96**, 241111(R) (2017).

[43] S. P. Mukherjee and J. P. Carbotte, Doping and tilting on optics in noncentrosymmetric multi-Weyl semimetals, Phys. Rev. B **97**, 045150 (2018).

[44] L. Lepori, M. Burrello, and E. Guadagnini, Axial anomaly in multi-Weyl and triple-point semimetals, J. High Energy Phys. 06 (2018) 110.

[45] R. Shankar, Renormalization-group approach to interacting fermions, Rev. Mod. Phys. **66**, 129 (1994).

[46] A. Damascelli, Z. Hussain, and Z.-X. Shen, Angle-resolved photoemission studies of the cuprate superconductors, Rev. Mod. Phys. **75**, 473 (2003).

[47] T. Valla, A. V. Fedorov, P. D. Johnson, B. O. Wells, S. L. Hulbert, Q. Li, G. D. Gu, and N. Koshizuka, Evidence for quantum critical behavior in the optimally doped cuprate $Bi_2Sr_2CaCu_2O_{8+\delta}$, Science **285**, 2110 (1999).

[48] A. Kaminski, M. Randeria, J. C. Campuzano, M. R. Norman, H. Fretwell, J. Mesot, T. Sato, T. Takahashi, and K. Kadowaki, Renormalization of Spectral Line Shape and Dispersion Below T_c in $Bi_2Sr_2CaCu_2O_{8+\delta}$, Phys. Rev. Lett. **86**, 1070 (2001).

[49] P. Richard, T. Sato, K. Nakayama, S. Souma, T. Takahashi, Y.-M. Xu, G. F. Chen, J. L. Luo, N. L. Wang, and H. Ding, Angle-Resolved Photoemission Spectroscopy of the Fe-Based $Ba_{0.6}K_{0.4}Fe_2As_2$ High Temperature Superconductor: Evidence for An Orbital Selective Electron-Mode Coupling, Phys. Rev. Lett. **102**, 047003 (2009).

[50] H. Miao, Z. P. Yin, S. F. Wu, J. M. Li, J. Ma, B.-Q. Lv, X. P. Wang, T. Qian, P. Richard, L.-Y. Xing, X.-C. Wang, C. Q. Jin, K. Haule, G. Kotliar, and H. Ding, Orbital-differentiated coherence-incoherence crossover identified by photoemission spectroscopy in LiFeAs, Phys. Rev. B **94**, 201109(R) (2016).

[51] D. A. Siegel, C.-H. Park, C. Hwang, J. Deslippe, A. V. Fedorov, S. G. Louie, and A. Lanzara, Many-body interactions in quasi-freestanding graphene, Proc. Natl. Acad. Sci. USA **108**, 11365 (2011).

[52] Z.-H. Pan, A. V. Fedorov, D. Gardner, Y. S. Lee, S. Chu, and T. Valla, Measurement of An Exceptionally Weak Electron-Phonon Coupling on the Surface of the Topological Insulator Bi_2Se_3 Using Angle-Resolved Photoemission Spectroscopy, Phys. Rev. Lett. **108**, 187001 (2012).

[53] N. Xu, C. E. Matt, E. Pomjakushina, X. Shi, R. S. Dhaka, D. C. Plumb, M. Radović, P. K. Biswas, D. Evtushinsky, V. Zabolotnyy, J. H. Dil, K. Conder, J. Mesot, H. Ding, and M. Shi, Exotic Kondo crossover in a wide temperature region in the topological Kondo insulator SmB_6 revealed by high-resolution ARPES, Phys. Rev. B **90**, 085148 (2014).

[54] T. Kondo, M. Nakayama, R. Chen, J. J. Ishikawa, E.-G. Moon, T. Yamamoto, Y. Ota, W. Malaeb, H. Kanai, Y. Nakashima, Y. Ishida, R. Yoshida, H. Yamamoto, M. Matsunami, S. Kimura, N. Inami, K. Ono, H. Kumigashira, S. Nakatsuji, L. Baltents, and S. Shin, Quadratic Fermi node in a 3D strongly correlated semimetal, Nat. Commun. **6**, 10042 (2015).

[55] J. González, F. Guinea, and M. A. H. Vozmediano, Marginal-Fermi-liquid behavior from two-dimensional Coulomb interaction, Phys. Rev. B **59**, 2474(R) (1999).

[56] J. Hofmann, E. Barnes, and S. Das Sarma, Why does Graphene Behave as a Weakly Interacting System? Phys. Rev. Lett. **113**, 105502 (2014).

[57] P. Goswami and S. Chakravarty, Quantum Criticality between Topological and Band Insulators in 3+1 Dimensions, Phys. Rev. Lett. **107**, 196803 (2011).

[58] P. Hosur, S. A. Parameswaran, and A. Vishwanath, Charge Transport in Weyl Semimetals, Phys. Rev. Lett. **108**, 046602 (2012).

[59] R. E. Throckmorton, J. Hofmann, E. Barnes, and S. Das Sarma, Many-body effects and ultraviolet renormalization in three-dimensional Dirac materials, Phys. Rev. B **92**, 115101 (2015).

[60] E.-G. Moon, C. Xu, Y. B. Kim, and L. Balents, Non-Fermi-Liquid and Topological States with Strong Spin-Orbit Coupling, Phys. Rev. Lett. **111**, 206401 (2013).

[61] I. F. Herbut and L. Janssen, Topological Mott Insulator in Three-Dimensional Systems with Quadratic Band Touching, Phys. Rev. Lett. **113**, 106401 (2014).

[62] B.-J. Yang, E.-G. Moon, H. Isobe, and N. Nagaosa, Quantum criticality of topological phase transitions in three-dimensional interacting electronic systems, Nat. Phys. **10**, 774 (2014).

[63] Y. Huh, E.-G. Moon, and Y. B. Kim, Long-range Coulomb interaction in nodal-ring semimetals, Phys. Rev. B **93**, 035138 (2016).

[64] H. Isobe, B.-J. Yang, A. Chubukov, J. Schmalian, and N. Nagaosa, Emergent Non-Fermi-Liquid at the Quantum Critical Point of a Topological Phase Transition in Two Dimensions, Phys. Rev. Lett. **116**, 076803 (2016).

[65] J.-R. Wang, G.-Z. Liu, and C.-J. Zhang, Excitonic pairing and insulating transition in two-dimensional semi-Dirac semimetals, Phys. Rev. B **95**, 075129 (2017).

[66] C.-Z. Chen, H. Liu, H. Jiang, and X. C. Xie, Positive magnetoconductivity of Weyl semimetals in the ultraquantum limit, Phys. Rev. B **93**, 165420 (2016).

[67] S.-M. Huang, S.-Y. Xu, I. Belopolski, C.-C. Lee, G. Chang, T.-R. Chang, B. Wang, N. Alidoust, G. Bian, M. Neupane, D. Sanchez, H. Zheng, H.-T. Jeng, A. Bansil, T. Neupert, H. Lin, and M. Z. Hasan, New type of Weyl semimetal with quadratic double Weyl fermions, Proc. Natl. Acad. Sci. USA **113**, 1180 (2016).

[68] Q. Liu and A. Zunger, Predicted Realization of Cubic Dirac Fermion in Quasi-One-Dimensional Transition-Metal Monochalcogenides, Phys. Rev. X **7**, 021019 (2017).

[69] D. C. Elias, R. V. Gorbachev, A. S. Mayorov, S. V. Morozov, A. A. Zhukov, P. Blake, L. A. Ponomarenko, I. V. Grigorieva, K. S. Novoselov, F. Guinea, and A. K. Geim, Dirac cones reshaped by interaction effects in suspended graphene, Nat. Phys. **7**, 701 (2011).

[70] J. Chae, S. Jung, A. F. Young, C. R. Dean, L. Wang, Y. Gao, K. Watanabe, T. Taniguchi, J. Hone, K. L. Shepard, P. Kim, N. B. Zhitenev, and J. A. Stroscio, Renormalization of the Graphene Dispersion Velocity Determined from Scanning Tunneling Spectroscopy, Phys. Rev. Lett. **109**, 116802 (2012).

[71] G. L. Yu, R. Jalil, B. Belle, A. S. Mayorov, P. Blake, F. Schedin, S. V. Morozov, L. A. Ponomarenko, F. Chiappini, S. Wiedmann, U. Zeitler, M. I. Katsnelson, A. K. Geim, K. S. Novoselov, and D. C. Elias, Interaction phenomena in graphene seen through quantum capacitance, Proc. Natl. Acad. Sci. USA **110**, 3282 (2013).

[72] J. Crossno, J. K. Shi, K. Wang, X. Liu, A. Harzheim, A. Lucas, S. Sachdev, P. Kim, T. Taniguchi, K. Watanabe, T. A. Ohki, and K. C. Fong, Observation of the Dirac fluid and the breakdown of the Wiedemann-Franz law in graphene, Science **351**, 1058 (2016).

[73] Z. K. Liu, J. Jiang, B. Zhou, Z. J. Wang, Y. Zhang, H. M. Weng, D. Prabhakaran, S.-K. Mo, H. Peng, P. Dudin, T. Kim, M. Hoesch, Z. Fang, X. Dai, Z. X. Shen, D. L. Feng, Z. Hussain, and Y. L. Chen, A stable three-dimensional topological Dirac semimetal Cd_3As_2, Nat. Mater. **13**, 677 (2014).

[74] C.-Z. Li, L.-X. Wang, H. Liu, J. Wang, Z.-M. Liao, and D.-P. Yu, Giant negative magnetoresistance induced by the chiral anomaly in individual Cd_3As_2 nanowires, Nat. Commun. **6**, 10137 (2015).

[75] C. Faugeras, S. Berciaud, P. Leszczynski, Y. Henni, K. Nogajewski, M. Orlita, T. Taniguchi, K. Watanabe, C. Forsythe, P. Kim, R. Jalil, A. K. Geim, D. M. Basko, and M. Potemski, Landau Level Spectroscopy of Electron-Electron Interactions in Graphene, Phys. Rev. Lett. **114**, 126804 (2015).

[76] J. Ruan, S.-K. Jian, H. Yao, H. Zhang, S.-C. Zhang, and D. Xing, Symmetry-protected ideal Weyl semimetal in HgTe-class materials, Nat. Commun. **7**, 11136 (2016).

[77] J. Ruan, S.-K. Jian, D. Zhang, H. Yao, H. Zhang, S.-C. Zhang, and D. Xing, Ideal Weyl Semimetals in the Chalcopyrites $CuTlSe_2$, $AgTlTe_2$, $AuTlTe_2$ and $ZnPbAs_2$, Phys. Rev. Lett. **116**, 226801 (2016).

[78] S. Nie, G. Xu, F. B. Prinz, and S.-C. Zhang, Topological semimetal in honeycomb lattice LnSI, Proc. Natl. Acad. Sci. USA **114**, 10596 (2017).

[79] Y. Du, E.-J. Kan, H. Xu, S. Y. Savrasov, and X. Wan, Turning copper metal into a Weyl semimetal, Phys. Rev. B **97**, 245104 (2018).

[80] D. E. Sheehy and J. Schmalian, Quantum Critical Scaling in Graphene, Phys. Rev. Lett. **99**, 226803 (2007).

[81] F. Setiawan and S. Das Sarma, Temperature-dependent many-body effects in Dirac-Weyl materials: Interacting compressibility and quasiparticle velocity, Phys. Rev. B **92**, 235103 (2015).